DOI: 10.1002/chem.200701910

The Mechanism of the (Bispidine)copper(II)-Catalyzed Aziridination of Styrene: A Combined Experimental and Theoretical Study

Peter Comba,* Carolin Lang, Carlos Lopez de Laorden, Amsaveni Muruganantham, Gopalan Rajaraman, Hubert Wadepohl, and Marta Zajaczkowski[a]

Abstract: Experimental and DFT-based computational results on the aziridination mechanism and the catalytic activity of (bispidine)copper(I) and -copper(II) complexes are reported and discussed (bispidine = tetra- or pentadentate 3,7-diazabicyclo[3.1.1]-nonane derivative with two or three aromatic N donors in addition to the two tertiary amines). There is a correlation between the redox potential of the copper(II/I) couple and the activity of the catalyst. The most active catalyst studied, which has the most positive redox potential among all (bispidine)-copper(II) complexes, performs 180 turnovers in 30 min. A detailed hybrid density functional theory (DFT) study provides insight into the structure, spin state, and stability of reactive intermediates and transition states, the oxidation state of the copper center, and the denticity of the nitrene source. Among the possible pathways for the formation of the aziridine product, the stepwise formation of the two N–C bonds is shown to be preferred, which also follows from experimental results. Although the triplet state of the catalytically active copper nitrene is lowest in energy, the two possible spin states of the radical intermediate are practically degenerate, and there is a spin crossover at this stage because the triplet energy barrier to the singlet product is exceedingly high.

Keywords: aziridination · copper · density functional calculations · N ligands · reaction mechanisms · styrene

Introduction

The development of methods for the efficient and enantioselective functionalization of alkenes by transition-metal-mediated oxygen transfer is an area of intense research,[1,2] and reactions such as the dihydroxylation and epoxidation of unfunctionalized alkenes have had a tremendous impact, specifically in the field of asymmetric synthesis.[3–5] Despite the importance of aziridines in organic synthesis and as biologically active natural products, the aziridination reaction catalyzed by transition metals has been less exploited.[6–9] There is increasing interest in aziridine synthesis in recent years, and the most promising route is the transition-metal-mediated addition of nitrenes to olefins.[10] Although there are examples of very efficient systems based on ruthenium porphyrine and manganese porphyrine complexes,[11,12] copper catalysts are often superior to other systems (Scheme 1),[13,14] and [*N*-(*p*-toluenesulfonyl)imino]phenyliodinane (PhINTs)[15] is the most frequently used but expensive nitrene source. Others, like chloroamine T,[16] are cheaper but less reactive.

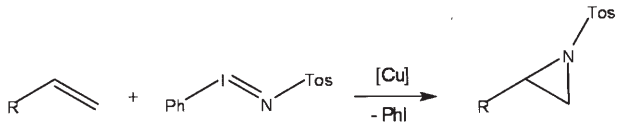

Scheme 1. The copper-catalyzed aziridination reaction of styrene. Tos = *p*-toluenesulfonyl.

A number of mechanistic details of the transition-metal-assisted aziridination reaction are still unclear, and, dependent on the catalyst, there might be different pathways. Hammett structure–reactivity studies on some copper catalysts have been reported, which support the involvement of a radical intermediate,[17,18] but other systems do not.[19–22] All attempts to trap and characterize radical intermediates

[a] Prof. Dr. P. Comba, C. Lang, Dr. C. Lopez de Laorden, A. Muruganantham, Dr. G. Rajaraman, Prof. Dr. H. Wadepohl, M. Zajaczkowski
Universität Heidelberg, Anorganisch-Chemisches Institut
INF 270, 69120 Heidelberg (Germany)
Fax: (+49)-6226–546617
E-mail: peter.comba@aci.uni-heidelberg.de

Supporting information for this article is available on the WWW under http://www.chemeurj.org/ or from the author.

have failed so far,[14,23] and there is no common mechanistic model that can account for the multitude of experimental observations and computational data. Experimental and computational results support the idea of a discrete nitrene intermediate and, with copper(I) as the catalytically active species, the formation of a copper(I) nitrene or an imidocopper(III) complex have been proposed.[18] However, copper(II) nitrene complexes and the activation of the nitrene source without electron transfer have been suggested as alternatives.[24] Often, the copper catalysts can be used in their +1 or +2 oxidation states.[14] If copper(II) is used, it was proposed to be reduced by PhINTs in the first step of the catalytic cycle.[18] Therefore, the redox potential of the copper(II) precatalyst may be correlated with the reactivity.

The copper catalysts discussed herein are based on tetra- and pentadentate bispidine ligands (3,7-diazabicyclo[3.3.1]-nonane derivatives, see Scheme 2). The extremely rigid ligand backbone and the moderate elasticity of the coordination geometry (which imply a flat potential-energy surface with steep walls),[25,26] together with a high complementarity of the ligands towards various metal ions, copper(II) in particular,[26,27] lead to outstanding properties of transition-metal bispidine complexes.[21] Based on a variety of aromatic N donors that are substituted to the bispidine backbone, a

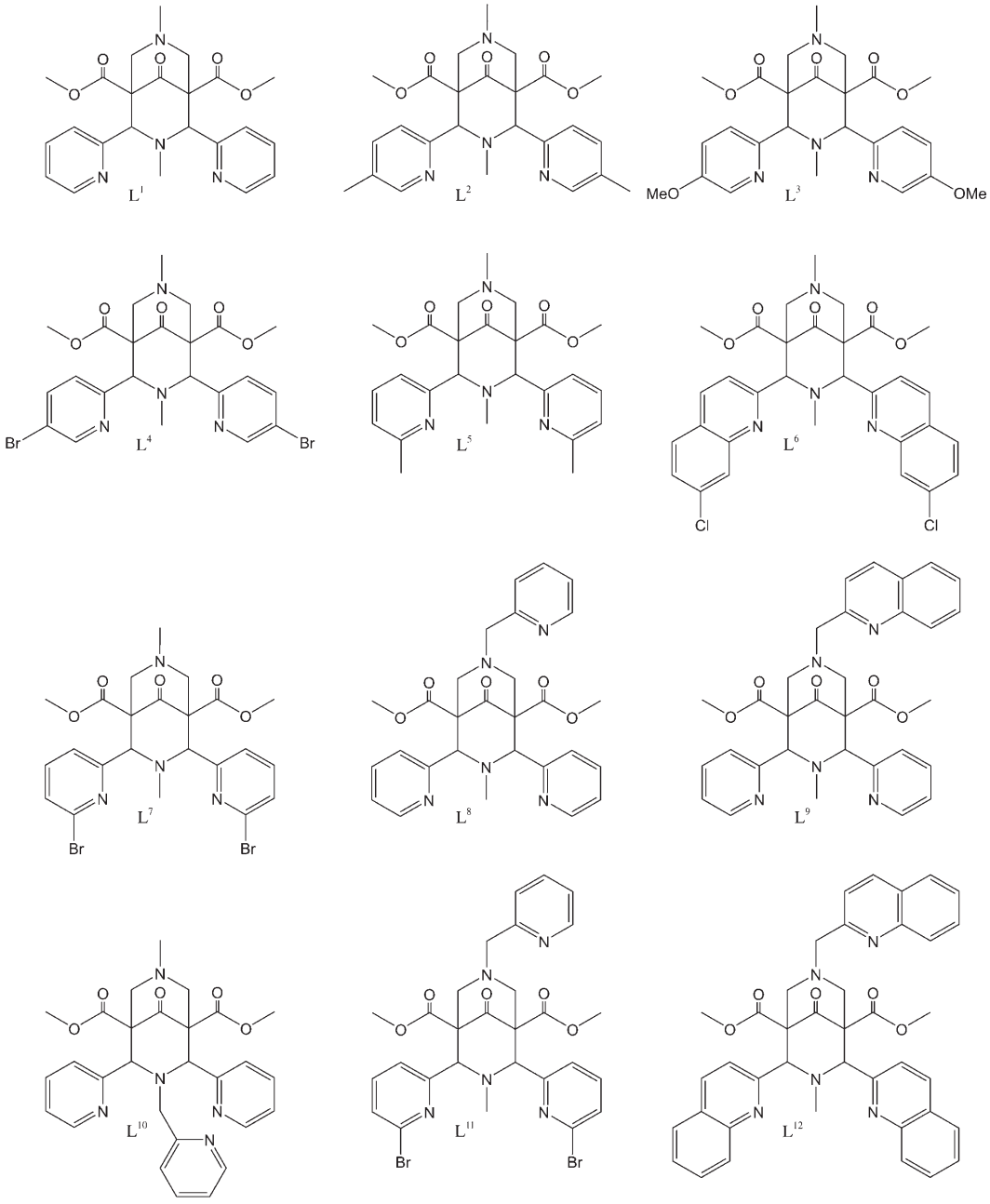

Scheme 2. Bispidine ligand structures.

range of copper(II) complexes with similar structures but strikingly different properties, for example, redox potentials, is available.[22] This series of complexes, together with some new derivatives, is used in the experimental part of this study to more thoroughly understand the (bispidine)copper-catalyzed aziridination reaction. The experimentally determined reactivities are supported by hybrid density functional theory (DFT) calculations.

Previous DFT calculations were performed on simple model systems with bi- and tetradentate ligand systems.[18,20,28] These results, together with the electronic and structural properties of some intermediates, provide important information about possible pathways but are not unambiguous and not necessarily relevant for our systems. With the tetradentate bispidine ligands, the addition of PhINTs may lead to a penta- or hexacoordinate intermediate (mono- or bidentate coordination mode of PhINTs), and the copper-catalyzed aziridination reaction may involve the concerted addition of the nitrene or proceed via a stepwise pathway with a radical intermediate. It therefore seemed appropriate to perform a detailed computational study to support our experimental data and to develop a model that might help to further improve the performance of the (bispidine)copper(II)-catalyzed aziridination reaction.

Results and Discussion

Syntheses, structures and solution properties of the (bispidine)copper(II) complexes: All tetra- and pentadentate bispidine ligands were prepared, according to a general procedure, by two consecutive Mannich reactions,[21,29] and the syntheses of L^1, L^5, L^8, and L^{10} have been published elsewhere (see Schemes S1–S3 in the Supporting Information for details of the ligand syntheses).[23,30] L^7 and L^{11} as well as the corresponding piperidone precursor pL^7 were obtained in acceptable yields from commercially available reactants. The amine component for L^9 and L^{12}, 2-(aminomethyl)quinoline, was prepared in two steps from 2-quinolinecarbaldehyde in 50% overall yield.[31] For the other new bispidines, the aldehyde components were not commercially available and different routes were used for their syntheses. 5-Methyl-2-pyridinecarbaldehyde for pL^2 and 5-bromo-2-pyridinecarbaldehyde for pL^4 were obtained through direct Br–Li exchange,[32] followed by a nucleophilic substitution with *N*,*N*-dimethylformamide (DMF). The *N*-oxide rearrangement route[33] was used for 5-methoxy-2-pyridinecarbaldehyde for pL^3, and for pL^6, the 7-chloro-2-quinolinecarbaldehyde was synthesized from 2-methyl-7-chloroquinoline by SeO_2 oxidation.[34] The copper(II) complexes of all ligands were obtained from equimolar amounts of a copper(II) salt and the ligand in acetonitrile under argon, followed by ether diffusion into the product solution to induce crystallization.

Crystals of X-ray quality were obtained for many of the complexes. Structural data, also including published structures,[23,25,30,35–37] are listed in Table 1, and the structural plots of the copper(II) complexes with the new ligands appear in Figure 1. With (bispidine)copper(II) complexes, isomers with Jahn–Teller-type elongations along one of the three axes (N7-Cu-X_{ax}, N3-Cu-X_{eq}, Ar1-Cu-Ar2) have been observed, and the stabilization of a particular geometry has been found to be a subtle combination of ligand-induced steric strain and electronic effects owing to the bispidine and the co-ligands.[21,36–38] The most commonly observed elongation is along the N7-Cu-X_{ax} axis, and for the tetradentate ligands, this geometry can be destabilized with sterically demanding substituents at the *ortho* position of the aromatic N donors (L^5, L^6, L^7).[36] Although there still is the usual elongation along N7–Cu with the "sterically innocent" monodentate co-ligand acetonitrile in combination with the methylated ligand L^5 or the less sterically demanding quinoline donors in L^6, larger co-ligands such as Cl^- ions lead to a partially quenched Jahn–Teller elongation along N3–Cu and, with the chelating NO_3^- ions, longer bonds to the aromatic donors are observed with L^5. With the large Br substituents of L^7, the latter type of structure is already observed with acetonitrile as the co-ligand. Similar trends are seen with the pentadentate ligands. The unsubstituted bispidine L^{10} induces two nearly degenerate minima that are similar to L^5 in the group of the tetradentate ligand in which the three possible isomeric structures are close in energy. Although, in general, there are three possible minima each with similar energy, their structures and therefore their properties (spectroscopic, electrochemical, reactivity) are

Table 1. Selected structural parameters of (bispidine)copper(II) complexes.[a]

Ligand	Co-ligand(s) X,Y (*trans*-N3, *trans*-N7)	Cu–N3 [Å]	Cu–N7 [Å]	Cu–N_{Ar1} [Å]	Cu–N_{Ar2} [Å]	Cu–X [Å]	Cu–Y [Å]	C-N3-C [°]
L^1[23]	$NCCH_3$, $OSO_2CF_3^-$	2.022(2)	**2.355(2)**	1.993(2)	1.998(2)	1.980(2)	**2.608(2)**	116.548
L^1[25]	NO_3^- bidentate	1.999(1)	**2.280(1)**	1.999(1)	1.999(1)	1.976(1)	**2.613(1)**	117.727
L^1[35]	Cl^-, –	2.042(3)	**2.272(3)**	2.020(3)	2.024(3)	2.232(1)	–	119.007
L^2	$NCCH_3$, –	2.007(1)	**2.244(1)**	1.992(1)	2.007(1)	1.966(1)	–	118.150
L^4	$NCCH_3$, BF_4^-	2.010(5)	**2.257(5)**	2.022(5)	2.020(5)	1.957(5)	**2.724(5)**	117.610
L^5[23]	$NCCH_3$, BF_4^-	2.004(4)	**2.376(4)**	2.052(4)	2.075(4)	1.950(5)	**2.911(4)**	117.688
L^5[23]	–, Cl^-	**2.147(3)**	2.120(3)	2.061(3)	2.064(3)	–	2.221(2)	119.630
L^5[36]	NO_3^- bidentate	1.987(2)	2.032(2)	**2.377(2)**	**2.376(2)**	1.982(2)	2.139(2)	114.642
L^6	$NCCH_3$, $NCCH_3$	1.987(1)	**2.370(2)**	2.124(1)	2.090(1)	1.967(2)	**2.634(2)**	116.700
L^7	$NCCH_3$, $NCCH_3/OH_2$	2.050(4)	2.103(4)	**2.441(4)**	**2.394(4)**	1.985(5)	2.051(4)[b]	112.100
L^8[30]	Py, Cl^-	2.036(2)	**2.368(2)**	2.028(2)	2.029(2)	2.029(2)	**2.717(1)**	117.160
L^{10}[37]	$NCCH_3$, Py	2.105(2)	2.106(2)	**2.260(2)**	**2.353(2)**	2.015(2)	2.027(2)	116.310
L^{10}[37]	H_2O, Py	2.058(3)	2.082(3)	**2.472(3)**	**2.330(3)**	1.972(3)	2.038(3)	113.970
L^{10}[37]	Cl^-, Py	2.070(2)	**2.478(2)**	2.011(2)	1.987(2)	2.255(1)	**2.544(2)**	117.420
L^{12}	q, $NCCH_3$	2.122(2)	2.014(2)	**2.288(2)**	**2.931(2)**	2.108(2)	1.988(3)	111.100

[a] The bold numbers denote elongated bonds. [b] Cu–N and Cu–O.

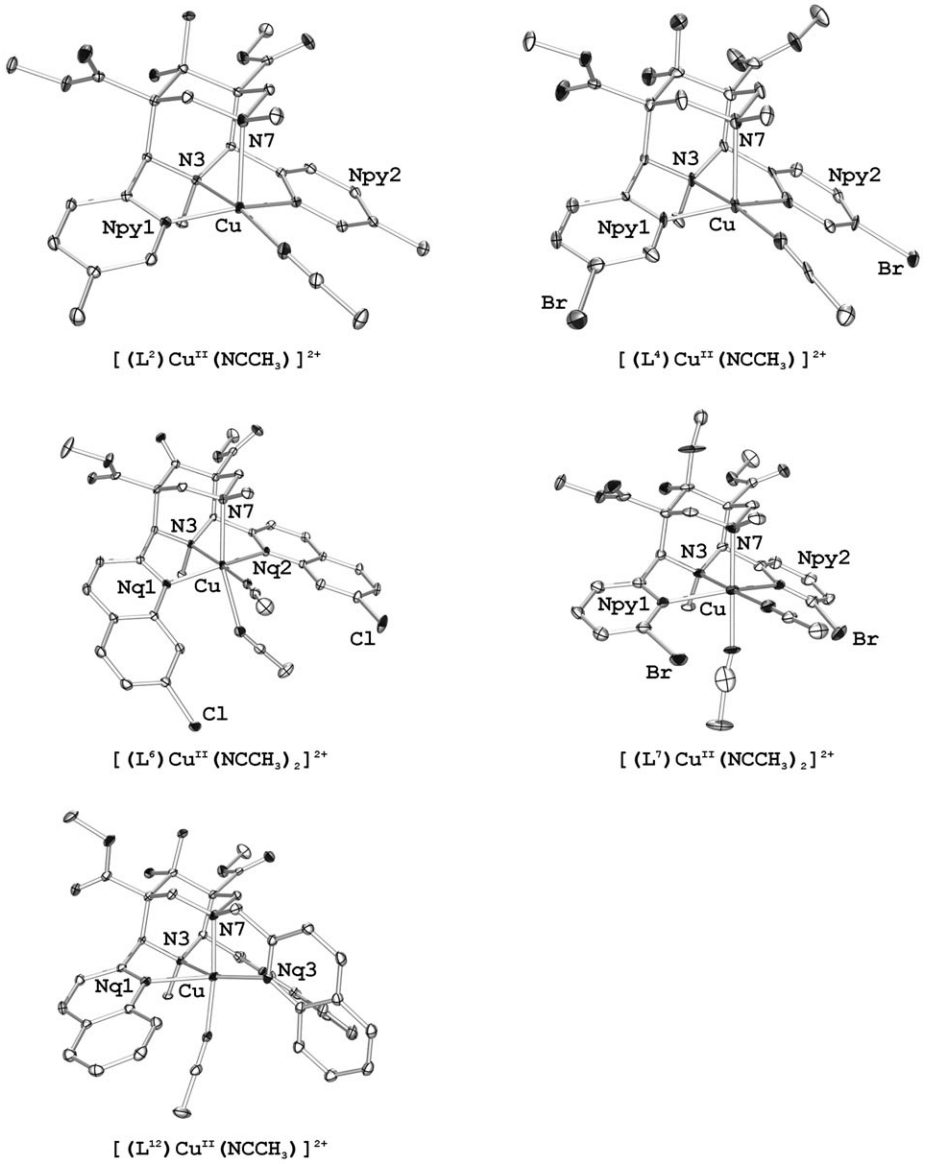

Figure 1. ORTEP plots of the new experimental structures of (bispidine)copper(II) complexes (ellipses shown at the 50% probability level); hydrogen atoms and counter ions are omitted for clarity.

of particular interest and will also be compared to the aziridination activities (see below). There is a rough correlation of the redox potentials with the (expected and observed) structural parameters (see also the computational section below). That is, for the copper(II) complexes of the tetradentate ligands L^5, L^6, and L^7, the structures with an elongation along the N7-Cu-X_{ax} axis are destabilized and they therefore have the highest redox potentials (the least stable copper(II) complexes). The dd transitions and spin Hamiltonian parameters (in particular $A_{\parallel}$) also follow this trend.[40] However, from the data, it also emerges that there are various effects that contribute to the structural and electronic properties.[41] Similar trends are observed for the complexes of the pentadentate ligands L^8 to L^{12}. Note that, in general, the complexes with the pentadentate ligands lead to more stable copper(II) complexes, which also follows from the redox potentials. However, of particular interest is the comparison of the complexes of the two isomeric ligands L^8 and L^{10} in which the spectroscopic and eletrochemical data suggest that there is a significant difference between the two isomers. This is also in agreement with the strikingly different. This has been observed and analyzed for L^5 and L^{10}.[36,37]

An interesting possibility emerging from these observations is to tune the electronic and, specifically, the electrochemical properties. That is, the destabilization of the preorganized "Jahn–Teller isomer" with an N7-Cu-X_{ax} elongation is the design principle used herein for the optimization of the aziridination reactivity (see the Introduction). A reduction of the Jahn–Teller stabilization energy by partial quenching of the elongation leads to a destabilization of the +2 oxidation state and therefore to the required increase of the redox potential. This assumption is supported by the corresponding stability constants and redox potentials.[21,27] The spectroscopic and electrochemical data of the copper(II) complexes of L^1–L^{12}, summarized in Table 2, are therefore

Table 2. Spectroscopic and electrochemical data of (bispidine)copper(II) complexes

Ligand	dd transitions in MeCN [nm]	Redox potential in MeCN vs. $AgNO_3$ [mV]	EPR data (DMF/H_2O 3:2) $g_{\parallel}$	$g_{\perp}$	$A_{\parallel}$
L^1	630	−413	2.245	2.072	172
L^2	624	−410	2.260	2.054	171
L^3	627	−387	2.260	2.056	173
L^4	633	−272	2.268	2.060	171
L^5	700	−94	2.245	2.085	165
L^6	735	+17	–	–	–
L^7	660	+53	2.305	2.065	156
L^8	625	−603	2.230	2.075	175
L^9	630	−552	2.198	2.042	173
L^{10}	665	−489	2.250	2.080	165
L^{11}	642	−389	2.258	2.055	168
L^{12}	632	−35	2.288	2.060	150

complex stabilities, and these have been discussed on the basis of structural features enforced by the ligands and the complementarity of the ligands with respect to copper(II).[27]

Aziridination experiments: The results of the (bispidine)-copper(II)-catalyzed aziridination of styrene are listed in Table 3. The reactions were all performed in dry acetonitrile (2 mL; 8.7 mmol of styrene) and generally at 25 °C. The catalyst/PhINTs/substrate ratio was 0.05:1:22 in most experiments. PhINTs is not soluble in acetonitrile and the reaction was considered to be finished when a clear solution was observed. Therefore, the reaction time, which was varied for different catalysts, is considered to be a measure of the reactivity of the catalysts. The yield of the aziridine product was determined by ^{1}H NMR spectroscopy with anthrone as the internal standard. This is considered to be a more precise method than the often-used technique of product isolation followed by a gravimetric analysis.[42] All reactions were carried out in dry solvents and under an inert atmosphere. For those reactions labeled specifically as "water-free", the complexes used were thoroughly dried.[43]

From the data, it emerges that there is a correlation between the redox potential of the (bispidine)copper(II) complexes and their efficiency as aziridination catalysts (see Tables 2 (redox potential) and 3 (reaction time)), and this is, in contrast with an earlier interpretation,[30] independent of the denticity of the bispidine used in the catalyst. The amount of product obtained (percentage yield or turn-over number) strongly depends on the reaction conditions and the particular ligand used. We assume that the reduced yields in some cases are due to cleavage of PhINTs into tosylamide and phenyl iodide, a reaction that is known to be catalyzed by copper(I).[13] Clearly, the rate ratio of the two reactions (aziridine formation vs. PhINTs degradation) depends on the catalyst. The side reaction may be suppressed to some extent under strictly water-free conditions as water serves as a proton source for the copper(I)-catalyzed cleavage of PhINTs.

$[(L^7)Cu(NCCH_3)_2](OTf)_2$ (OTf = triflate) is found to be the most active catalyst (reaction time). For this complex, we therefore studied the temperature dependence and varied the relative amounts of substrate and catalyst (Table 3, entries 8–10, 11–13, 14–17). The reaction is accelerated with increasing temperature. No significant effect is observed with respect to the yield, that is, the cleavage of PhINTs may not be suppressed at higher or lower temperatures. A reduction of the excess of styrene to five equivalents does not change the yield of aziridination product, but the further reduction to a stoichiometric amount relative to PhINTs substantially reduces the yield, even after a very long reaction time. This indicates that the substrate may be involved in the rate-determining step of the catalytic cycle. A reduction in the amount of catalyst by a factor of 10 (0.5 vs. 5 mol %) does not significantly reduce the yield (but increases the turnover number). With a lower catalyst loading (0.1 mol %), the reaction gets much slower and full conversion of the PhINTs is not observed any more. Compared with recently published systems,[24,44] the (bispidine)copper(II) complexes, in particular $[(L^7)Cu(NCCH_3)_2]^{2+}$, are, under standard conditions, excellent aziridination catalysts for styrene.

The high activity of the L^7-based (bispidine)copper(II) complex is based on the most positive redox potential observed so far for (bispidine)copper(II) complexes. This appears to be a combination of the ligand-enforced geometry and electronic effects: 1) the sterically demanding Br atoms in the *ortho* position to the pyridine N-donor atoms prevent the coordination of co-ligands in the *trans* position to N3 with the expected usual $Cu-N_{Py}$ distance of around 2.0 Å; 2) the electron-withdrawing effect of the bromine substituents leads to a weakening of the nitrogen donors; therefore, the preferred elongation is along the Ar1-Cu-Ar2 axis, and coordination of substrates *trans* to N3 is then

Table 3. Aziridination of styrene with (bispidine)copper(II) complexes.

Entry	Ligand	Denticity	T [°C]	Equiv styrene (vs. PhINTs)	mol % cat. (vs. PhINTs)	Reaction time [h]	Yield [%]	TON[a]
1[b]	L^1	4	25	22	5	7	38.5 (73.0)	7.7 (14.6)
2	L^2	4	25	22	5	7	4.0	0.8
3	L^3	4	25	22	5	7	38.5	7.7
4	L^4	4	25	22	5	2	59.0	11.8
5[b]	L^5	4	25	22	5	2	35.0 (51.5)	7.0 (10.3)
6	L^6	4	25	22	5	2	55.5	11.1
7[b]	L^7	4	25	22	5	0.5	80.5 (94.0)	16.1 (18.8)
8[c]	L^7	4	50	22	5	0.1	91.0	18.2
9[c]	L^7	4	25	22	5	0.5	94.0	18.8
10[c]	L^7	4	0	22	5	1.5	93.0	18.6
11[c]	L^7	4	25	22	5	0.5	94.0	18.8
12[c]	L^7	4	25	5	5	0.5	90.5	18.1
13[c,d]	L^7	4	25	1	5	24	46.0	9.2
14[c]	L^7	4	25	22	5	0.5	94.0	18.8
15[c]	L^7	4	25	22	1	0.5	94.0	94
16[c]	L^7	4	25	22	0.5	0.5	90.0	180
17[c,d]	L^7	4	25	22	0.1	24	27.5	270
18[b,d] [30]	L^8	5	25	22	5	7	0 (1.0)	0 (0.2)
19	L^9	5	25	22	5	7	63.0	12.6
20[b,d] [30]	L^{10}	5	25	22	5	7	0 (9.0)	0 (1.8)
21	L^{11}	5	25	22	5	7	60.5	12.1
22[b]	L^{12}	5	25	22	5	2	68.5 (74.5)	13.7 (14.9)
23[c]	L^5	4	25	22	100	1	90.2	0.9
24[c,e]	L^5	4	25	22	5	24	3.5/7.5	0.70/1.50
25[c,e]	L^7	4	25	22	5	5	3.8/4.2	0.76/0.84

[a] TON = n(product)/n(catalyst). [b] Yields for absolutely water-free conditions shown in parentheses. [c] Water-free conditions. [d] Incomplete conversion. [e] reaction with *cis*-β-methylstyrene; yields and TON of *cis*/*trans* product

less hindered; 3) the reduced nucleophilicity of the Br-substituted pyridine donors leads to a reduced ligand field and therefore to a destabilization of the copper(II) oxidation state.

The reduction of the copper(II) precatalyst by PhINTs might occur by an inner- or an outer-sphere process. To probe this experimentally, a stoichiometric reaction (catalyst/PhINTs = 1:1) was performed with one of the copper(II) precatalysts. This experiment with $[(L^5)Cu(NCCH_3)](OTf)_2$ shows a fast conversion (clear solution after 10 min) with a high yield (around 90%, see Table 3, entry 23). This indicates that the reduction of the copper(II) atom to the active copper(I) species by PhINTs is an inner-sphere process; in the case of an outer-sphere reduction, the nitrene source would be deactivated and this would lead to very small yields. To further probe the reaction mechanism, the catalytic aziridination of *cis*-β-methylstyrene was studied with $[(L^5)Cu(NCCH_3)](OTf)_2$ and $[(L^7)Cu(NCCH_3)_2](OTf)_2$. In both reactions, a mixture of *cis* and *trans* products was observed (see Table 3, entries 24 and 25). This is typical for a radical mechanism in which the two C–N bonds are formed in a stepwise and not in a concerted process.

In contrast with all other bispidine catalysts, within the first few seconds after the addition of PhINTs, the reduction of $[(L^7)Cu(NCCH_3)_2]^{2+}$ can be visually observed by a color change of the reaction mixture from light blue to yellow green. In situ UV/Vis spectroscopy shows a reduction of the copper(II) dd transitions and, in addition, a new charge-transfer band at 308 nm is observed. This differs from the spectrum of $[(L^7)Cu(NCCH_3)]^+$, which has a charge-transfer transition at 340 nm. The UV/Vis spectrum of a mixture of $[(L^7)Cu(NCCH_3)]^+$ and PhINTs has, as expected, the same band at 308 nm. This indicates that PhINTs is coordinated to $\{(L^7)Cu\}^+$ to form the active nitrene species, and it supports the postulated inner-sphere reduction of the copper(II) precatalyst by PhINTs. For steric reasons, the coordination of PhINTs is assumed to occur *trans* to N7 (see above).

The electronic structure of copper(III) nitrenes: Our computational studies are primarily based on copper complexes with L^5, which was the most active catalyst in the preliminary studies,[30] and has a significant reactivity among the systems presented herein. Based on our experimental (see above) and published theoretical observations,[18,20,30] Scheme 3 was adopted for the DFT calculations. In the initial step, the $\{(L^5)Cu^I\}$ catalyst reacts with PhINTS to form an $\{(L^5)Cu^I$-PhINTs$\}$ complex. Homolytic cleavage of the N–I bond produces the nitrene $\{(L^5)Cu^I$-NTs$\}$. There is experimental evidence that copper(III) nitrenes are the catalytically active species in various copper-catalyzed aziridina-

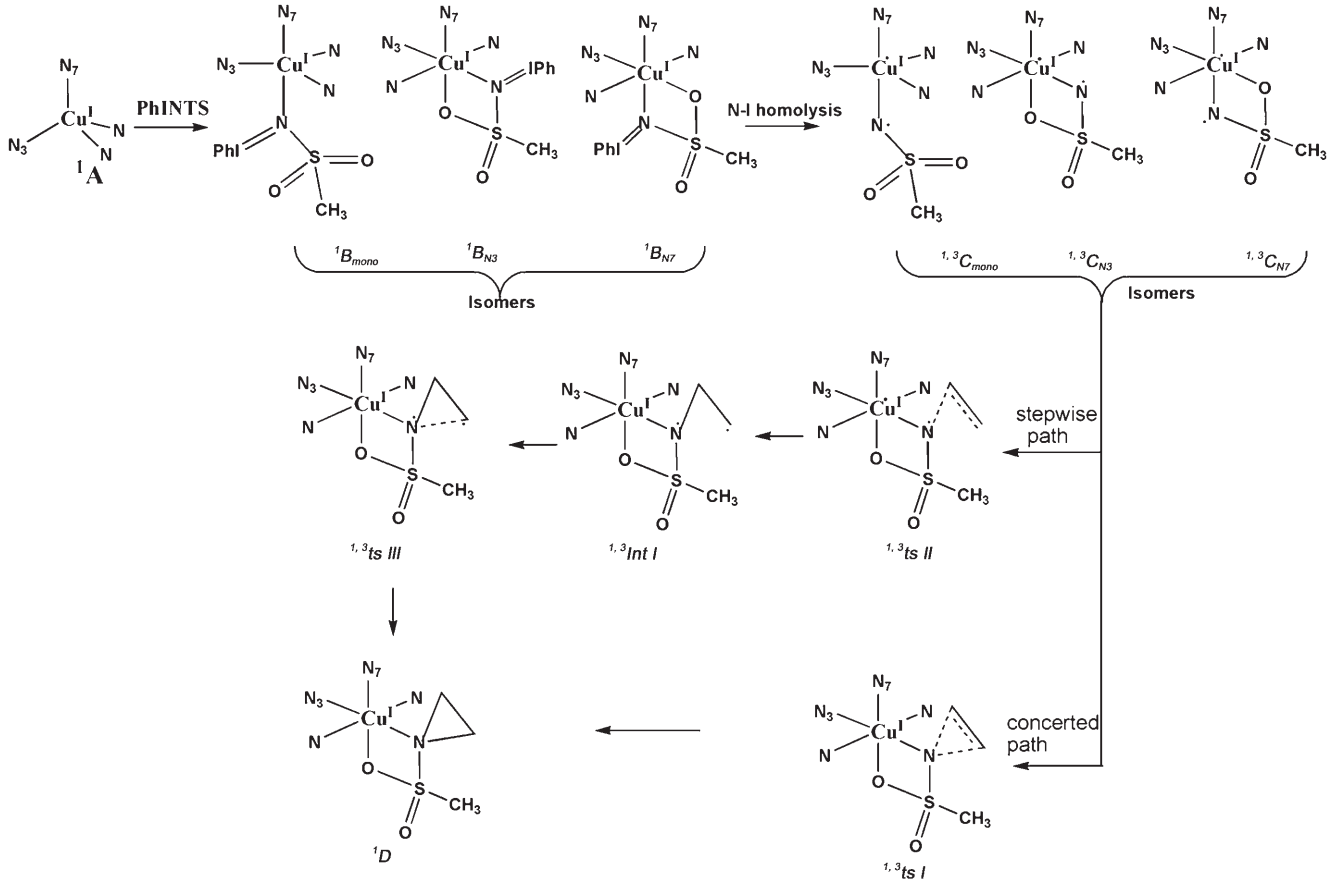

Scheme 3. Mechanistic pathways of the copper(I)-catalyzed aziridination reaction.

tion reactions.[45–47] Therefore, we first focus on the electronic structure and energetics of the nitrene complexes.

With the tetradentate ligand L^5-based system, there are two possible coordination modes, mono- and bidentate. Depending on the catalyst, both modes are possible. With the tetradentate bispidine complexes, there are two isomers each for the mono- and bidentate coordination modes (see Scheme 3), and we have computed all possible isomers and compared their energies. For the monodentate coordination mode, the substrate-*trans*-to-N7 isomer is, as expected for steric reasons, more stable, and therefore, we have only considered this *trans*-N7 isomer with a monodentate nitrene (see Scheme 3, $^{1,3}\boldsymbol{C}_{mono}$). For the bidentate coordination mode, the two isomers (nitrene-*trans*-to-N3 ($^{1,3}\boldsymbol{C}_{N3}$); nitrene-*trans*-to-N7 ($^{1,3}\boldsymbol{C}_{N7}$)) have similar stabilities.

There are two possible spin states, a triplet and a singlet, and both have been computed for all isomers considered. In all cases, the triplet is found to be the ground state. The unpaired electrons in the $^{3}\boldsymbol{C}_{mono}$ structure are orthogonal to each other, that is, the triplet state is stabilized by exchange coupling. The energy gap to the corresponding singlet state is 13.5 kJ mol^{-1}. The $^{3}\boldsymbol{C}_{N3}$ isomer is higher in energy with a margin of 19.0 kJ mol^{-1}, and the $^{3}\boldsymbol{C}_{N7}$ isomer lies at 22.3 kJ mol^{-1}. The DFT-optimized structures of the three triplet nitrene species are shown in Figure 2, and selected structural parameters and energies for both spin states are given in Table 4. The $^{1,3}\boldsymbol{C}_{mono}$ complexes are distorted trigonal bipyramidal (N3-Cu-$N_{nitrene}$ = 124.2°) with a Cu–$N_{nitrene}$ distance of 1.919 Å in the triplet and 1.931 Å in the singlet state. These bonds are slightly longer than that in a (μ-N_{Ar})-dicopper(II) complex (1.794 and 1.808 Å)[46] but in the range of those computed in other similar studies.[18,20] The optimized bond lengths involving the copper bispidine fragment are in the expected range (see Table 4).[21] The geometries of the $^{1,3}\boldsymbol{C}_{N3}$ and $^{1,3}\boldsymbol{C}_{N7}$ isomers are distorted octahedral, and one of the "axial" pyridine bonds each is strongly elongated (3.14 and 3.19 Å in the triplet states). The Cu–$N_{nitrene}$ distances in the $^{3}\boldsymbol{C}_{N3}$ and $^{3}\boldsymbol{C}_{N7}$ isomers are 1.95 and 1.97 Å, and those in the corresponding singlet states are slightly shorter with 1.89 and 1.90 Å, respectively.

The spin density plots for $^{3}\boldsymbol{C}_{mono}$, $^{3}\boldsymbol{C}_{N3}$, and $^{3}\boldsymbol{C}_{N7}$ are given in Figure 2. The unpaired electron on the nitrene nitrogen atom is delocalized to the $d_{x^2-y^2}$ orbital of the copper center, that is, the bonding in the triplet state may be described as Cu^{II}–N$^{\bullet}$. In the singlet state, the unpaired electrons on copper and nitrogen are antiferromagnetically coupled. A second singlet state, which may be described as Cu^{III}=N has much higher energies (111.5, 19.6, and 17.9 kJ mol^{-1} for $\boldsymbol{C}_{mono}$, $\boldsymbol{C}_{N3}$, and $\boldsymbol{C}_{N7}$, respectively). The corresponding wavefunction stability tests reveal an internal instability with respect to the open-shell singlet described above. Therefore, the corresponding spin surface is ignored for the further studies.

The aziridination reaction mechanism: Our experimental results suggest that the copper(II) complexes are less reactive than the copper(I) catalysts.[30] Moreover, as indicated above (see Table 2 and 3), the aziridination reactivities are correlated with the redox potentials of the catalysts in which

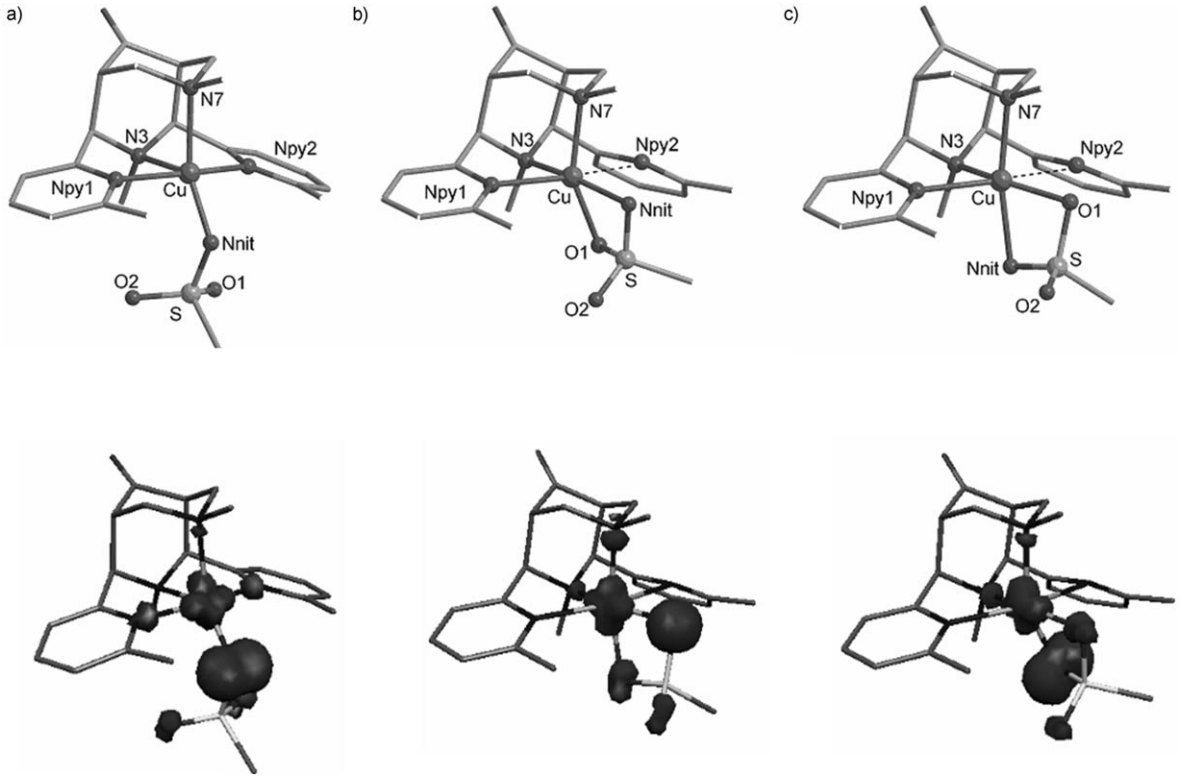

Figure 2. DFT-optimized structures and computed spin density plots of a) $^{3}\boldsymbol{C}_{mono}$, b) $^{3}\boldsymbol{C}_{N3}$, and c) $^{3}\boldsymbol{C}_{N7}$ with L^5 (see Scheme 3; N_{nit} = $N_{nitrene}$).

Table 4. Selected B3LYP-computed structural parameters of the reactants, intermediates, and products in the aziridination mechanism of the $Cu^{I}L^{5}$ catalyst.

	^1A + PhINTS	^1B	$^1C_{mono}$	$^3C_{mono}$	$^1C_{N3}$	$^3C_{N3}$	$^1C_{N7}$	$^3C_{N7}$	$^1ts\ II$	$^3ts\ II$	$^1int\ I$	$^3int\ I$	$^1ts\ III$	$^3ts\ III$	^1D
energy [kJ mol^{-1}]	0.0	−28.8	−84.3	−97.9	−67.5	−78.9	−65.6	−75.6	27.6	14.2	−73.0	−71.5	−34.7	41.2	155.7
bond lengths [Å]															
Cu−N7	2.119	2.013	2.197	2.193	2.024	2.075	2.046	2.067	2.050	2.056	2.071	2.072	2.0798	2.088	2.074
Cu−N3	2.199	2.020	2.190	2.198	2.020	2.054	2.007	2.058	2.084	2.091	2.055	2.055	2.105	2.109	2.149
Cu−N_{Py1}	1.950	2.579	2.087	2.089	2.965	2.268	3.045	2.284	2.565	2.632	3.060	3.062	2.362	2.944	3.612
Cu−N_{Py2}	1.950	2.949	2.087	2.089	2.515	3.143	2.461	3.199	2.850	2.910	2.423	2.425	2.963	2.393	2.033
Cu−O	–	1.891	3.459	3.471	1.923	2.156	1.932	2.136	1.927	1.930	2.062	2.056	2.091	1.971	3.160
Cu−$N_{nitrene}$	–	1.870	1.931	1.919	1.895	1.945	1.910	1.966	2.004	2.026	2.025	2.025	2.104	2.051	2.019
$N_{nitrene}$−C1	–	–	–	–	–	–	–	–	1.913	2.185	1.477	1.477	1.453	1.456	1.501
$N_{nitrene}$−C2	–	–	–	–	–	–	–	–	2.569	2.565	2.516	2.511	2.164	1.932	1.497
valence angles [°]															
N3-Cu-$N_{nitrene}$	–	171.9	125.0	124.2	171.7	148.0	95.4	96.7	165.8	158.7	163.7	163.1	155.7	159.5	129.0
N7-Cu-$N_{nitrene}$	–	95.2	148.4	149.2	96.2	97.3	169.9	151.4	101.3	101.6	106.9	107.0	106.0	106.4	120.5
Cu-$N_{nitrene}$-S	–	94.4	118.1	118.9	95.0	93.9	94.6	92.8	92.2	91.9	94.3	94.3	90.3	90.9	115.6

the most active (bispidine)copper complexes have the least negative reduction potentials (Figure 3). As reported previously[30] and supported by our experiments, it is assumed that the copper(II) PhINTS precursors undergo innersphere electron transfer in which the N−I bond cleaves homolytically to produce $PhI^{+\bullet}$ and the copper(I) catalyst.

The initial step in the catalytic cycle therefore is coordination of PhINTs to the (bispidine)copper(I) complex. The formation of the three possible isomers $^1B_{mono}$, $^1B_{N3}$, and $^1B_{N7}$ is exothermic with reaction energies of 28.8, 29.5, and 28.3 kJ mol^{-1}, respectively. The Cu−$N_{nitrene}$ distances are shorter than in the corresponding copper nitrenes (1.89, 1.87, 1.88 Å in $^1B_{mono}$, $^1B_{N3}$, $^1B_{N7}$, respectively), and the N−IPh bonds are elongated from 2.02 Å in PhINTs to 3.89, 3.34, and 3.39 Å in $^1B_{mono}$, $^1B_{N3}$, $^1B_{N7}$ (plots of the optimized structures are given in the Supporting Information). An attempt to add ethylene as a substrate to these intermediates results in the cleavage of the N−I bonds. That is, the formation of the nitrene intermediate is a nearly barrierless reaction and a Lewis acid mechanism can therefore be excluded. Similar observations emerge from other computational and also from experimental studies.[18,45] The homolytic cleavage of the N=I bond produces the nitrenes C and PhI. The monodentate isomer $^3C_{mono}$ is the lowest in energy; in the precursor ^1B, the three isomers are nearly degenerate and the lowest-energy path is from $^1B_{N3}$ to $^3C_{mono}$ with a reaction energy of −68.4 kJ mol^{-1}.

There are two pathways for the addition of an olefin to $^{1,3}C$ to produce the aziridine product complex, that is, stepwise (radical intermediate) or concerted (symmetric transition state). Relaxed potential-energy scans at BS1 (type of basis set, see the Experimental Section) were used to find transition states in both pathways (variation of the C−N distances from 2.7 to 1.7 Å with a step size of 0.1 Å; the corresponding plots are given in the Supporting Information).

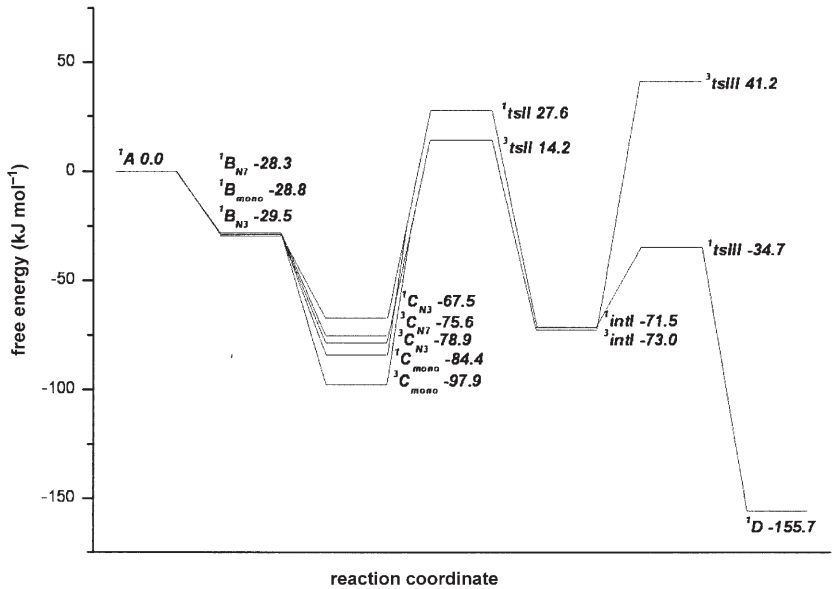

Figure 3. Computed potential-energy diagram of the aziridination reaction with $[Cu^{I}L^{5}]^{+}$.

Starting with the pentacoordinate isomers $^{1,3}C_{mono}$, there is an isomerization to the corresponding $^{1,3}C_{N3}$ isomers along the reaction coordinate. The energy difference between the nitrenes $^{1,3}C_{mono}$ and $^{1,3}C_{N3}$ isomers is only 19.0 and 16.9 kJ mol^{-1} on the triplet and singlet surfaces, respectively, and the energy barrier for rotation around the $N_{nitrene}$−S single bond is low. We therefore only consider the *trans*-N3 isomer surfaces.

A concerted mechanism on the triplet spin surface is unlikely owing to the required electronic reorganization (see Figure 4). It therefore is not unexpected that optimization of

the maximum energy point of the corresponding relaxed energy scan leads to the transition state of the stepwise mechanism ***^{3}tsII***. Optimization of the maximum-energy point on the singlet surface also yielded the structure of ***^{1}tsII***, that is, an asynchronous concerted transition state, which collapsed to the radical intermediate ***^{1}intI***. We therefore have neglected a concerted mechanism. Incidentally, the experimental studies resulted in the same conclusion (see above).

The first reaction in the stepwise mechanism is the formation of the radical intermediate ***^{1,3}intI***. The singlet–triplet energy gap of the nitrene ***C_{N3}*** is only 11.4 kJ mol^{-1} with the triplet as the ground state. Therefore, both spin surfaces were computed.[48] The results from the stepwise path are collected in the energy profile diagram of Figure 3. Structural data of ***^{1,3}tsII*** are listed in Table 4 and a plot of the optimized structure of the more stable triplet state structure ***^{3}tsII*** is shown in Figure 5. On the singlet and triplet surfaces, the alkene approaches the nitrene reactive center from the open side above the Cu/N_{Py1}/N_{Py2}/N3-plane and the N_{Py1}–Cu direction (note that this is the shorter N_{Py}–Cu bond with a larger N_{Py}-Cu-$N_{nitrene}$ angle, 121.0 vs. 86.5° in the triplet state). The Cu–$N_{nitrene}$ bonds on the triplet and singlet surfaces are elongated with respect to the ***C_{N3}*** intermediates (2.026 vs. 1.945 Å, 2.004 vs. 1.913 Å, respectively) and the new $N_{nitrene}$–C1 bonds are much shorter than the bonds to the second ethylene carbon atom $N_{nitrene}$···C2, which clearly shows the asymmetry of the transition state on the way to a radical intermediate (2.185 vs. 2.565 Å and 1.913 vs. 2.569 Å for the triplet and singlet states, respectively). The energy barriers on the triplet and singlet surfaces are comparable (93.1 vs. 95.1 kJ mol^{-1}) and the corresponding products (***^{3}intI***, ***^{1}intI***) are nearly degenerate (see Figure 3). A spin-density plot of ***^{3}tsII*** is given in Figure 6 and the spin densities of the intermediates and transition states on both spin surfaces are given in the Supporting Information. In the triplet state, the spin density on copper does not vary much as a result of the interaction with ethylene, although there is some propagation of spin density from copper to the coordinated sulfonate oxygen through spin delocalization. The spin density on the nitrene site is significantly reduced in ***^{3}tsII*** and transferred to the ethylene substrate through spin polarization, which induces a significant radical character to the olefin substrate and therefore indicates that it is a product-like transition state.

The two spin states of ***intI*** (parallel or antiparallel alignment of the unpaired electron on the $N_{nitrene}$ and the radical carbon atom C1) are degenerate (triplet ground state with a 1.5 kJ mol^{-1} margin; this is clearly within the error of the DFT method used). This is not unexpected because in ***intI***, the unpaired electrons are exchange coupled (see Figure 4). The optimized structure of the ***^{3}intI*** is shown in Figure 6 (that of ***^{1}intI*** is basically identical) and selected structural parameters for both spin states are given in Table 4. The N–C bond is fully formed in the radical intermediate (1.477 Å in both spin states) and the Cu–$N_{nitrene}$ distance is unchanged from the transition state.

Ring closure from the radical intermediate ***^{1,3}intI*** to the product ***^{1,3}D***, that is, the aziridine coordinated to copper(I), proceeds via transition state ***^{1,3}tsII***. On the triplet surface, this involves a spin reversal (see Figure 4), and ***^{3}tsII*** has therefore an exceedingly high energy (activation barrier of 114.3 kJ mol^{-1} relative to ***^{3}intI*** compared with a barrier of 36.8 kJ mol^{-1} on the singlet surface). Structural parameters and energies of all relevant species are listed in Table 4 and structural plots of ***^{1}tsIII*** and ***^{1}D*** are presented in Figure 5 (spin densities are tabulated in the Supporting Information). The formation of the $N_{nitrene}$–C2 bond is evident in both spin states. There is an elongation of the copper–nitrene bond and, in particular on the triplet surface, there is a strengthening of the Cu–O and an elongation of the $N_{nitrene}$–S bond. The product (***^{1}D***) has fully formed N–C1,C2 bonds and a

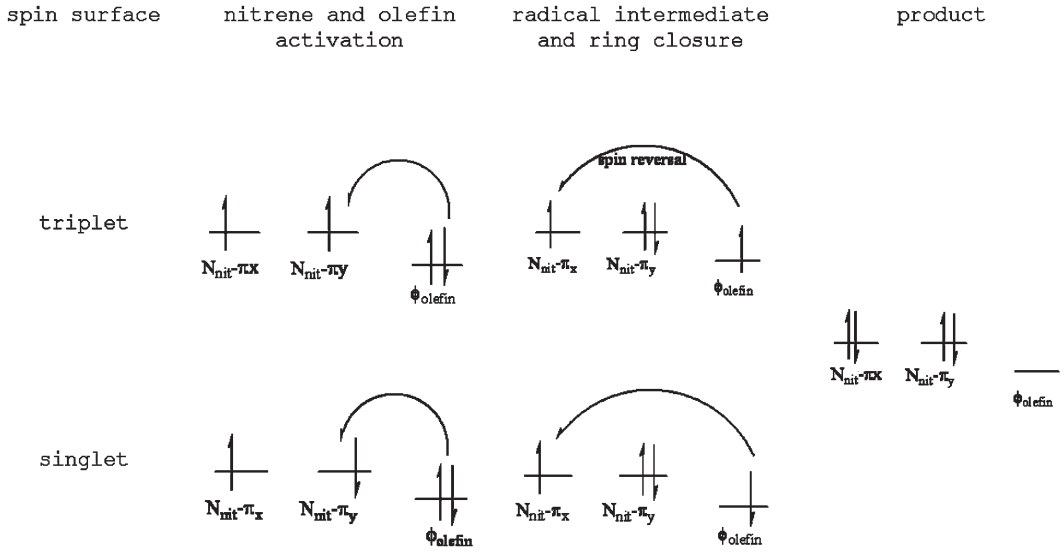

Figure 4. Electronic reorganization for the aziridination reaction on the singlet and triplet spin surfaces. ($N_{nit} = N_{nitrene}$.)

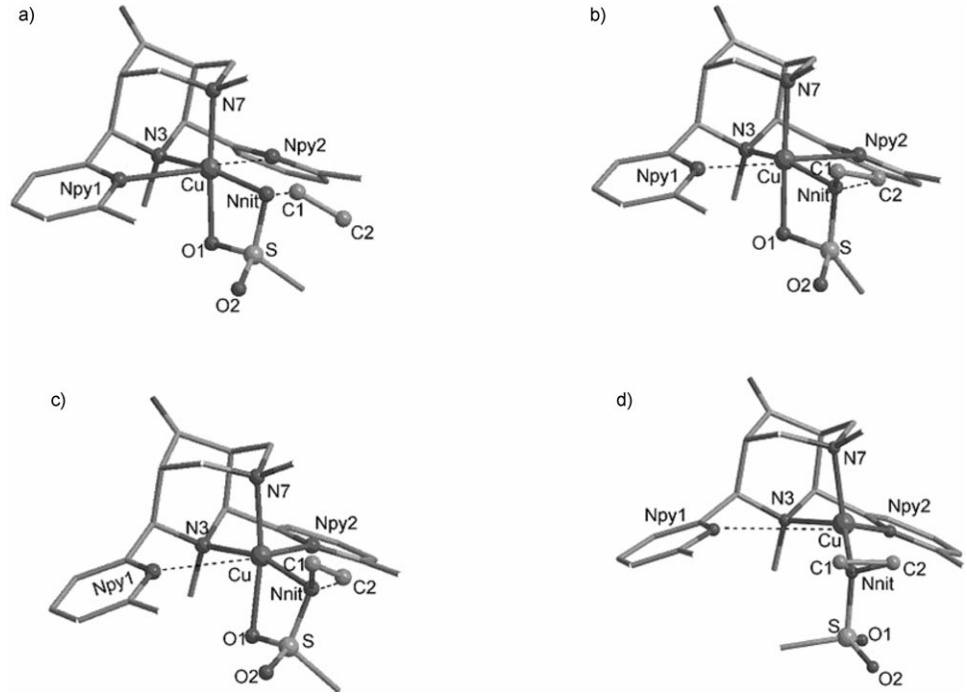

Figure 5. DFT-optimized structures of a) ^{3}***tsII***, b) ^{3}***intI***, c) ^{3}***tsIII***, and d) ^{1}***D***, each with L^5 (see Scheme 3; $N_{nit} = N_{nitrene}$).

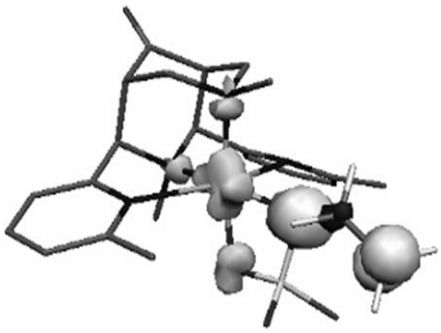

Figure 6. Computed spin-density plot of ^{3}***tsII*** with L^5.

very weak Cu–O interaction. Dissociation of the Cu–$N_{nitrene}$ and regeneration of the catalyst to close a catalytic cycle is slightly endothermic by 18.6 kJ mol^{-1}.

Interesting features in the stepwise mechanism are that the first transition state on both the singlet and triplet surfaces differ only by approximately 13 kJ mol^{-1} and the subsequent formation of the radical intermediates also have very similar reaction energies on both the surfaces. Therefore, our calculations suggest a two-state reactivity in which the reaction pathway to the radical intermediate will involve both spin states. The two-state reactivity can also explain the selectivity observed by some specific substrates: substrates that stabilize the radical intermediates will react via triplet and singlet states whereas substrates that are not capable of stabilizing the radical intermediates will selectively react with the singlet nitrene through a concerted mechanism to yield enantioselective products.

The radical intermediate has a triplet ground state, thus no spin crossing is required until formation of the radical intermediate. However, the barrier height for the second transition state on the triplet surface is substantial compared with that of the singlet, which indicates a possible spin-crossover scenario before the formation of the transition state. The product formation is thermodynamically favorable. Therefore, the reaction at the second step is expected to occur exclusively on the singlet surface. The very small energy difference and similar geometries of the two forms suggest that an interconversion between the singlet and triplet state is a facile process. Therefore, we did not compute the minimum-energy crossing point (MECP) in this case.

The aziridination reaction with copper(II) complexes: The reaction of the copper(II) precatalysts and PhINTs without innersphere electron transfer produces the ^{2}***B*$_{mono}$, ^{2}***B*$_{N3}$, and ^{2}***B*$_{N7}$ precursors in an exothermic process with reaction energies of 32.5, 27.7, and 26.6 kJ mol^{-1}, respectively, which is similar to those of the copper(I) precursors. Homolytic cleavage of the N–I bond forms the putative copper(IV) nitrenes. There are two different possible spin states, a high-spin quartet and a low-spin doublet. The optimized structures, selected bond lengths, and computed spin densities are given in the Supporting Information. The ^{4}***C*$_{N3}$ and ^{4}***C*$_{N7}$ isomers have Cu–$N_{nitrene}$ distances of 2.073 and 2.130 Å, respectively, and the structure of ^{4}***C*$_{mono}$ is similar to that of ^{3}***C*$_{mono}$, the copper nitrene, with a N3-Cu-$N_{nitrene}$ angle of 121.8°. The complex ^{2}***C*$_{mono}$ is the lowest in energy with the quartet state at 9.7 kJ mol^{-1} and ^{2}***C*$_{N3}$, with a bidentate nitrene, 44.8 kJ mol^{-1} higher in energy. However, compared with the copper(III) nitrenes (copper(I) pathway), the copper(IV) nitrenes (copper(II) pathway) have exceedingly high potential-energy barriers (see the Supporting Information). Therefore, the copper(II) nitrene pathway can be excluded because the formation of copper(I) nitrenes from copper(II) PhINTs by heterolytic cleavage of the PhI moiety (copper(I) nitrene and $PhI^{\cdot+}$) is more exothermic. After the formation of the copper(I) nitrene, the reaction follows the same pathway as for the copper(I) precursor. This is also consistent with our experimental observation (see the section on Aziridination Experiments) and previous

theoretical studies. To this end, our calculations suggest that the mechanism of N–I bond cleavage is related to the oxidation state of the copper center, resulting in a homolytic cleavage for the copper(I) precursor and heterolytic cleavage for the copper(II) precatalyst.

Penta- versus tetradentate bispidine ligands: The experimental data suggest that the pentadentate bispidine copper(II)-complexes generally have more negative redox potentials (more stable copper(II) complexes).[30] However, it appears that those pentadentate systems with comparably high redox potentials (e.g. L^{11}, L^{12}) lead to similar reactivities to those with tetradentate ligands and that there is a general correlation based on the redox potentials (e.g., L^3 vs. L^4, L^5 vs. L^{12}). This suggests that, in the reactive copper(I) state, one of the bispidine donors may dissociate and a bidentate PhINTs then leads to the same type of intermediate as discussed with the tetradentate bispidine ligands. This is not unexpected and is supported by NMR spectroscopy and DFT calculations of (bispidine)copper(I) complexes.[49,50] We therefore have not done any additional computational studies for these systems.

Conclusion

Based on the original assumption that the copper(II) precatalysts are reduced by PhINTs to copper(I),[30] we have been able to optimize our (bispidine)copper(II) aziridination catalysts. This was achieved by tuning the reduction potential on the basis of subtle structural modifications, which enforce a stabilization of the less-common "Jahn–Teller isomers".[36–38] Both experimental and DFT-based results indicate that the reduction of the copper(II) precursors is an inner-sphere process to yield a catalytically active copper nitrene species. In contrast with earlier results,[30] there is no significant difference between complexes of tetra- and pentadentate bispidine ligands. L^7, which has the most positive redox potential among the (bispidine)copper(II) complexes known so far, has the highest activity. From the fact that both tetra- and pentadentate ligands may lead to active catalysts, it emerges that mono- and bidentate coordination of PhINTs may be of importance, and this also follows from the DFT studies. The experimental observation that a radical intermediate is involved in the catalytic aziridination of *cis*-β-methylstyrene is nicely supported by the DFT calculations, which indicate that in the rate-determining first step, the reaction of the copper nitrene with the olefin leads to a radical intermediate, which in the second step is cyclized to the coordinated aziridine.

Experimental Section

Materials and measurements: Chemicals and absolute solvents (Aldrich, Fluka) were used without further purification. Styrene was degassed and kept for five minutes over molecular sieves (4 Å) before being used in the aziridination experiments. 5-Methoxy-2-pyridinecarbaldehyde and 7-chloro-2-quinolinecarbaldehyde were synthesized as reported in the literature.[33,34] The other aldehyde and amine components were commercially available, except for the components described beneath. Electronic spectra were measured on a Jasco V-570 instrument. NMR spectra were recorded at 200 MHz (^{1}H) and 50.3 MHz (^{13}C) on a Bruker AS-200 instrument with the solvent as the internal reference. EPR measurements were performed on a Bruker ELEXSYS-E-500 instrument at 125 K, and the spin Hamiltonian parameters were obtained by simulation of the spectra with XSophe.[51,52] For the electrochemical measurements, a BAS-100B workstation with a three-electrode setup consisting of a glassy-carbon working electrode, a Pt wire as the auxiliary electrode, and an Ag/$AgNO_3$ reference electrode (0.01 M Ag^+, 0.1 M $(Bu_4N)(BF_4)$ in MeCN) was used. The solutions were purged with N_2 before the measurements; scan rate 100 mV s^{-1}. The redox potentials are reported with respect to $Ag/AgNO_3$. The mass spectra were measured on a Finnigan 8400 instrument; nibeol = 4-nitrobenzyl alcohol. Elemental analyses were performed in the analytical laboratories of the chemical institutes at the University of Heidelberg.

Syntheses

5-Bromo-2-pyridinecarbaldehyde: A solution of BuLi (2.5 M in hexanes, 10.0 mL, 25.3 mmol) was slowly added to a solution of 2,5-dibromopyridine (5 g, 21.1 mmol) in toluene (250 mL) at −78 °C and the mixture was stirred for 2 h. Then DMF (2.15 mL, 27.6 mmol) was added. After stirring for 1 h at −78 °C, the solution was warmed up to −10 °C and quenched with saturated NH_4Cl aqueous solution at this temperature. The organic phase was separated, the solvent removed in vacuo and the pure product obtained by column chromatography (silica gel, hexane/ethyl acetate 9:1, $R_f = 0.2$) in 35 % yield. ^{1}H NMR (200 MHz, $CDCl_3$): $\delta = 7.85$ (d, 1H, $^3J_{H,H} = 8.3$ Hz, Ar–H), 8.03 (d, 1H, $^3J_{H,H} = 8.3$ Hz, Ar–H), 8.86 (br s, 1H, Ar–H), 10.04 ppm (s, 1H, CHO).

5-Methyl-2-pyridinecarbaldehyde: A solution of BuLi (2.5 M in hexanes, 14.0 mL, 34.9 mmol) was slowly added to a solution of 2-bromo-5-methylpyridine (5 g, 29.1 mmol) in toluene (350 mL) at −78 °C and the mixture was stirred for 2 h. Then DMF (2.90 mL, 37.8 mmol) was added. After stirring for 1 h at −78 °C, the solution was warmed up to −10 °C and quenched with saturated NH_4Cl aqueous solution at this temperature. The organic phase was separated, the solvent was removed in vacuo and the pure product was obtained by column chromatography (silica gel, hexane/ethyl acetate 7:3, $R_f = 0.2$) in 35 % yield. ^{1}H NMR (200 MHz, $CDCl_3$): $\delta = 2.44$ (s, 3H, CH_3), 7.67 (dd, 1H, $^3J_{H,H} = 7.9$ Hz, $^4J(H,H) = 0.7$ Hz, Ar–H), 7.88 (d, 1H, $^3J_{H,H} = 7.9$ Hz, Ar–H), 8.61 (d, 1H, $^4J_{H,H} = 0.7$ Hz, Ar–H), 10.05 ppm (s, 1H, CHO).

2-(Aminomethyl)quinoline: A solution of 2-quinolinecarbaldehyde (5.00 g, 30.9 mmol) in ethanol (150 mL) was added to a solution of hydroxylamine hydrochloride (2.14 g, 30.9 mmol) and potassium carbonate (4.95 g, 35.8 mmol) in water (25 mL). The mixture was refluxed for 30 min. After cooling down, the yellowish precipitate was filtered, washed with water, and dried in vacuo to yield 71 % product. The 2-formaldoximoquinoline (2.00 g, 11.6 mmol) was dissolved in trifluoroacetic acid (23 mL). Zink powder (4.25 g, 65 mmol) was added slowly. The mixture was stirred at room temperature for 1 h and then poured into a mixture of aqueous sodium hydroxide solution (2 M, 200 mL) and chloroform (100 mL) under ice cooling. The organic phase was washed with brine, dried over $MgSO_4$, and the solvent was removed in vacuo to obtain the product in 71 % yield. ^{1}H NMR (200 MHz, $CDCl_3$): $\delta = 2.60$ (br s, 2H, NH_2), 4.16 (2, 2H, CH_2), 7.30–8.15 ppm (m, 6H, Ar–H).

The piperidones pL^1, pL^5, pL^{10}, and pL^{12} were synthesized according to published methods.[22,23,30]

General piperidone synthesis: To a solution of two equivalents of the corresponding aldehyde and one equivalent dimethyl 1,3-acetonedicarboxylate in methanol, 1.2 equivalents of the corresponding amine was added slowly under ice cooling. After some hours stirring at room temperature, a white/yellow precipitate was formed, which was filtered, washed with methanol, and dried in vacuo.

1-Methyl-2,6-bis(5-methylpyridin-2-yl)-4-oxopiperidine-3,5-dicarboxylic acid dimethyl ester pL^2: Following the general piperidone synthesis, 5-methyl-2-pyridinecarbaldehyde (1.55 g, 12.8 mmol), 41 % aqueous meth-

ylamine solution (0.65 mL, 7.7 mmol), and dimethyl 1,3-acetonedicarboxylate (0.92 mL, 6.4 mmol) in methanol (5 mL) gave the product in 34% yield. ^{1}H NMR (200 MHz, $CDCl_3$, keto form): δ = 1.73 (s, 3H, CH_3–N), 2.30 (s, 6H, CH_3–Ar), 3.63 (s, 6H, Ar–OCH_3), 4.41 (d, 2H, $^3J_{H,H}$ = 11.2 Hz, CH), 4.59 (d, 2H, $^3J_{H,H}$ = 11.2 Hz, CH), 7.30–7.55 (m, 4H, Ar–H), 8.32–8.40 ppm (m, 2H, Ar-H); ^{13}C NMR ($CDCl_3$; keto form): δ = 18.2 (2C, Ar–CH_3), 33.7 (1C, CH_3–N), 52.0 (2C, OCH_3), 57.6 (2C, CH–N), 69.8 (2C, CH–CO), 123.9, 132.6, 137.3, 149.4, 154.5 (10C, C_{Ar}), 168.6 (2C, $COOCH_3$), 200.7 ppm (1C, C=O); MS-FAB (nibeol) *m/z*: 412.2 [*M*]; elemental analysis calcd (%): C 64.22, H 6.12, N 10.21; found: C 64.31, H 6.10, N 10.27.

2,6-Bis(5-methoxypyridin-2-yl)-1-methyl-4-oxopiperidine-3,5-dicarboxylic acid dimethyl ester pL^3: Following the general piperidone synthesis, 5-methoxy-2-pyridinecarbaldehyde (0.80 g, 5.8 mmol), 41% aqueous methylamine solution 0.30 mL, 3.5 mmol), and dimethyl 1,3-acetonedicarboxylate (0.42 mL, 2.9 mmol) in methanol (3 mL) gave the product in 27% yield. ^{1}H NMR (200 MHz, CDCl3$_3$, keto form): δ = 1.80 (s, 3H, CH_3–N), 3.70 (s, 6H, Ar–OCH_3), 3.92 (s, 6H, OCH_3), 4.48 (d, 2H, $^3J_{H,H}$ = 11.3 Hz, CH), 4.64 (d, 2H, $^3J_{H,H}$ = 11.3 Hz, CH), 7.27 (dd, 2H, $^3J_{H,H}$ = 8.5 Hz, $^4J_{H,H}$ = 2.7 Hz, Ar–H), 7.49 (d, 2H, $^3J_{H,H}$ = 8.5 Hz, Ar–H), 8.31 ppm (d, 2H, $^4J_{H,H}$ = 2.7 Hz, Ar–H); ^{13}C NMR ($CDCl_3$; keto form): δ = 25.5 (1C, CH_3–N), 52.0 (2C, OCH_3), 55.5 (2C, Ar–OCH_3), 57.7 (2C, CH–N), 67.9, 69.3 (2C, CH–CO), 121.3, 124.7, 136.2, 149.4, 155.0 (10C, C_{Ar}), 168.5 (2C, $COOCH_3$), 200.7 ppm (1C, C=O); MS-FAB (nibeol) *m/z*: 444.0 [*M*+H]; elemental analysis calcd (%): C 59.59, H 5.68, N 9.48; found: C 59.43, H 5.90, N 8.92.

2,6-Bis(5-bromopyridin-2-yl)-1-methyl-4-oxopiperidine-3,5-dicarboxylic acid dimethyl ester pL^4: Following the general piperidone synthesis, 5-bromo-2-pyridinecarbaldehyde (1.20 g, 6.5 mmol), 41% aqueous methylamine solution (0.33 mL, 3.9 mmol), and dimethyl 1,3-acetonedicarboxylate (0.47 mL, 3.2 mmol) in methanol (8 mL) gave the product in 66% yield. ^{1}H NMR (200 MHz, CDCl3$_3$, keto form): δ = 2.26 (s, 3H, CH_3–N), 3.63 (s, 3H, OCH_3), 3.73 (s, 3H, OCH_3), 4.10–4.30 (m, 1H, CH), 4.30–4.50 (m, 1H, CH), 4.79 (s, 1H, CH–N), 7.10–7.20 (m, 2H, Ar–H), 7.60–7.80 (m, 2H, Ar–H), 8.50–8.70 (m, 2H, Ar–H), 12.46 ppm (s, 1H, OH); ^{13}C NMR ($CDCl_3$; enol form): δ = 31.6 (1C, CH_3–N), 37.7 (1C, CH–N), 52.2, 52.7 (2C, OCH_3), 60.2 (C, CH–N), 97.7 (1C, C=COH), 124.1, 124.8, 125.7, 138.9, 139.1, 139.5, 149.7, 150.1, 150,3 (10C, C_{Ar}), 155.8 (1C, C=COH), 167.2, 168.4 ppm (2C, $COOCH_3$); MS-FAB (nibeol) *m/z*: 541.8 [*M*]; elemental analysis calcd (%): C 44.39, H 3.54, N 7.76; found: C 44.11, H 3.52, N 7.66.

2,6-Bis(7-chloroquinolin-2-yl)-1-methyl-4-oxopiperidine-3,5-dicarboxylic acid dimethyl ester pL^6: Following the general piperidone synthesis, 7-chloro-2-quinolinecarbaldehyde (5.40 g, 28.2 mmol), 41% aqueous methylamine solution 1.43 mL, 16.9 mmol), and dimethyl 1,3-acetonedicarboxylate (2.04 mL, 14.1 mmol) in methanol (20 mL) gave the product in 65% yield. ^{1}H NMR (200 MHz, CDCl3$_3$, keto form): δ = 1.78 (s, 3H, CH_3–N), 3.61 (s, 6H, Ar–OCH_3), 4.56 (d, 2H, $^3J_{H,H}$ = 11.2 Hz, CH), 5.21 (d, 2H, $^3J_{H,H}$ = 11.2 Hz, CH), 7.27–8.25 ppm (m, 10H, Ar–H); ^{13}C NMR ($CDCl_3$; keto form): δ = 30.7 (1C, CH_3–N), 51.8 (2C, OCH_3), 61.1 (2C, CH–N), 69.3 (2C, CH–CO), 125.7, 125.9, 127.5, 128.3, 128.6, 135.1, 136.1, 147.2, 158.4 (18C, C_{Ar}), 169.2 (2C, $COOCH_3$), 201.6 ppm (1C, C=O); MS-FAB (nibeol) *m/z*: 551.8 [*M*]; elemental analysis calcd (%): C 60.22, H 4.43, N 7.39; found: C 60.23, H 4.16, N 7.49.

2,6-Bis(6-bromopyridin-2-yl)-1-methyl-4-oxopiperidine-3,5-dicarboxylic acid dimethyl ester pL^7: Following the general piperidone synthesis, 6-bromo-2-pyridinecarbaldehyde (10.00 g, 53.8 mmol), 41% aqueous methylamine solution (2.73 mL, 32.3 mmol) and dimethyl 1,3-acetonedicarboxylate (3.88 mL, 26.9 mmol) in methanol (25 mL) gave the product in 82% yield. ^{1}H NMR (200 MHz, $CDCl_3$, enol form): δ = 2.26 (s, 3H, CH_3–N), 3.63 (s, 3H, OCH_3), 3.83 (s, 3H, OCH_3), 4.04 (d, 1H, $^3J_{H,H}$ = 9.6 Hz, CH), 4.50 (d, 1H, $^3J_{H,H}$ = 9.6 Hz, CH), 4.80 (s, 1H, CH–N), 7.26–7.62 (m, 6H, Ar–H), 12.46 ppm (s, 1H, OH); ^{13}C NMR ($CDCl_3$; enol form): δ = 31.6 (1C, CH_3–N), 37.7 (1C, CH–N), 52.2, 52.7 (2C, OCH_3), 60.2 (C, CH–N), 97.7 (1C, C=COH), 121.8, 123.0, 127.4, 138.6, 138.8, 139.1, 140.7, 140.8, 141.6, (10C, C_{Ar}), 158.4 (1C, C=COH), 168.8 ppm (2C, $COOCH_3$); MS-FAB (nibeol) *m/z*: 541.8 [*M*], elemental analysis calcd (%): C 44.39, H 3.54, N 7.76; found: C 44.39, H 3.53, N 7.77.

The bispidones L^1, L^5, L^8, and L^{10} were synthesized according to published methods.[22,23]

General bispidone synthesis: To a suspension of 1 equivalent piperidone in methanol or ethanol, 2.4 equivalents of a 37% aqueous formaldehyde solution and 1.2 equivalents of the corresponding amine were added at room temperature. The mixture was refluxed for 1 to 24 h. After the mixture was allowed to cool down, a white/yellow precipitate was formed, filtered, washed with methanol, and dried in vacuo.

3,7-Dimethyl-2,4-bis(5-methylpyridin-2-yl)-9-oxo-3,7-diazabicyclo[3.3.1]-nonane-1,5-dicarboxylic acid dimethyl ester L^2: Following the general bispidine synthesis, piperidone pL^2 (0.80 g, 1.9 mmol), formaldehyde solution (0.37 mL, 4.6 mmol), and 41% (0.18 mL, 2.3 mmol) aqueous methylamine solution in methanol(5 mL) gave the product in 49% yield. ^{1}H NMR ($CDCl_3$): δ = 1.99 (s, 3H, CH_3–N), 2.24 (s, 3H, CH_3–N), 2.31 (s, 6H, CH_3–Ar), 2.49 (d, 2H, $^2J_{H,H}$ = 12.0 Hz, H6/H8 equatorial, CH_2), 3.00 (d, 2H, $^2J_{H,H}$ = 12.0 Hz, H6/H8 axial, CH_2), 3.81 (s, 6H, OCH_3), 4.65 (s, 2H, H2/H4, CH), 7.56 (dd, 2H, $^3J_{H,H}$ = 8.0 Hz, $^4J_{H,H}$ = 2.0 Hz, Ar–H), 7.93 (d, 2H, $^3J_{H,H}$ = 8.0 Hz, Ar–H), 8.30–8.34 ppm (m, 2H, Ar–H); ^{13}C NMR ($CDCl_3$): δ = 18.2 (2C, Ar–CH_3), 43.0, 44.5 (2C, CH_3–N), 52.4 (2C, OCH_3), 60.7 (2C, CH_2–N), 62.2, (2C, C–CO), 73.6 (2C, CH–N), 123.0, 132.4, 137.0, 149.5, 155.9 (10C, C_{Ar}), 168.7 (2C, $COOCH_3$), 203.8 ppm (1C, C=O); MS-FAB (nibeol) *m/z*: 467.0 [*M*+H]; elemental analysis calcd (%): C 64.36, H 6.48, N 12.01; found: C 63.95, H 6.39, N 11.95.

2,4-Bis(5-methoxypyridin-2-yl)-3,7-dimethyl-9-oxo-3,7-diazabicyclo[3.3.1]-nonane-1,5-dicarboxylic acid dimethyl ester L^3: Following the general bispidine synthesis, piperidone pL^3 (0.75 g, 1.7 mmol), formaldehyde solution (0.31 mL, 4.1 mmol), and 41% aqueous methylamine solution (0.17 mL, 2.0 mmol) in methanol (6 mL) gave the product in 38% yield. ^{1}H NMR ($CDCl_3$): δ = 1.97 (s, 3H, CH_3–N), 2.26 (s, 3H, CH_3–N), 2.53 (d, 2H, $^2J_{H,H}$ = 12.5 Hz, H6/H8 equatorial, CH_2), 3.04 (d, 2H, $^2J_{H,H}$ = 12.5 Hz, H6/H8 axial, CH_2), 3.80 (s, 6H, Ar–OCH_3), 3.86 (s, 6H, -OCH_3), 4.64 (s, 2H, H2/H4, CH), 7.28 (dd, 2H, $^3J_{H,H}$ = 8.7 Hz, $^4J_{H,H}$ = 2.9 Hz, Ar–H), 7.93 (d, 2H, $^3J_{H,H}$ = 8.7 Hz, Ar–H), 8.18 ppm (d, 2H, $^4J_{H,H}$ = 2.9 Hz, Ar–H); ^{13}C NMR ($CDCl_3$): δ = 42.9, 44.5 (2C, CH_3–N), 52.4 (2C, OCH_3), 55.6 (2C, Ar–OCH_3), 60.7, 62.4 (2C, C–CO), 73.3 (2C, CH–N), 121.4, 123.9, 136.0, 150.8, 155.0 (10C, C_{Ar}), 168.7 (2C, $COOCH_3$), 203.8 ppm (1C, C=O); MS-FAB (nibeol) *m/z*: 499.0 [*M*]; elemental analysis calcd (%): C 59.52, H 6.27, N 10.89; found: C 59.35, H 6.02, N 11.14.

2,4-Bis(5-bromopyridin-2-yl)-3,7-dimethyl-9-oxo-3,7-diazabicyclo[3.3.1]-nonane-1,5-dicarboxylic acid dimethyl ester L^4: Following the general bispidine synthesis, piperidone pL^4 1.06 g (2.0 mmol), formaldehyde solution (0.35 mL, 4.7 mmol), and 41% aqueous methylamine solution (0.20 mL, 2.4 mmol) in methanol (4 mL) gave the product in 74% yield. ^{1}H NMR ($CDCl_3$): δ = 2.00 (s, 3H, CH_3-N), 2.23 (s, 3H, CH_3–N), 2.50 (d, 2H, $^2J_{H,H}$ = 12.8 Hz, H6/H8 equatorial, CH_2), 2.90 (d, 2H, $^2J_{H,H}$ = 12.8 Hz, H6/H8 axial, CH_2), 3.80 (s, 6H, OCH_3), 4.70 (s, 2H, H2/H4, CH), 7.92 (d, 2H, $^4J_{H,H}$ = 0.9 Hz, Ar–H), 7.94 (d, 2H, $^3J_{H,H}$ = 2.1 Hz, Ar–H), 8.56 ppm (dd, 2H, $^3J_{H,H}$ = 2.1 Hz, $^4J_{H,H}$ = 0.9 Hz, Ar–H); ^{13}C NMR ($CDCl_3$): δ = 43.2, 44.5 (2C, CH_3–N), 52.6 (2C, OCH_3), 60.6 (2C, CH_2–N), 61.8 (2C, C–CO), 73.1 (2C, CH–N), 120.1, 124.7, 139.2, 150.3, 157.4 (10C, C_{Ar}), 168.2 (2C, $COOCH_3$), 202.8 (1C, C=O); MS-FAB (nibeol) *m/z*: 596.6 [*M*+H]; elemental analysis calcd (%): C 44.97, H 4.27, N 9.12; found: C 45.37, H 4.24, N 9.15.

2,4-Bis(7-chloroquinolin-2-yl)-3,7-dimethyl-9-oxo-3,7-diazabicyclo[3.3.1]-nonane-1,5-dicarboxylic acid dimethyl ester L^6: Following the general bispidine synthesis, piperidone pL^6 (2.00 g, 3.6 mmol), formaldehyde solution (0.64 mL, 8.6 mmol), and 41% aqueous methylamine solution (0.37 mL, 4.3 mmol) in ethanol (15 mL) gave the product in 78% yield. ^{1}H NMR ($CDCl_3$): δ = 2.11 (s, 3H, CH_3–N), 2.28 (s, 3H, CH_3–N), 2.50 (d, 2H, $^2J_{H,H}$ = 12.2 Hz, H6/H8 equatorial, CH_2), 2.92 (d, 2H, $^2J_{H,H}$ = 12.2 Hz, H6/H8 axial, CH_2), 3.92 (s, 6H, OCH_3), 4.96 (s, 2H, H2/H4, CH), 7.51 (dd, 2H, $^3J_{H,H}$ = 8.6 Hz, $^4J_{H,H}$ = 2.1 Hz, Ar–H), 7.79 (d, 2H, $^3J_{H,H}$ = 8.6 Hz, Ar–H), 7.96 (d, 2H, $^4J_{H,H}$ = 2.1 Hz, Ar–H), 8.26 (d, 2H, $^3J_{H,H}$ = 8.6 Hz, Ar–H), 8.35 ppm (d, 2H, $^3J_{H,H}$ = 8.6 Hz, Ar–H); ^{13}C NMR ($CDCl_3$): δ = 43.6, 44.4 (2C, CH_3–N), 52.6 (2C, OCH_3), 61.0 (2C, CH_2–N), 62.3 (2C, C–CO), 74.0 (2C, CH–N), 120.9, 126.1, 127.8, 128.3, 128.7, 135.5, 136.3, 147.9, 160.8 (18C, C_{Ar}), 168.3 (2C, $COOCH_3$), 203.0 ppm (1C, C=O); MS-

FAB (nibeol) m/z: 606.9 [M]; elemental analysis calcd (%): C 60.40, H 4.74, N 9.09; found: C 60.58, H 4.53, N 8.94.

2,4-Bis(6-bromopyridin-2-yl)-3,7-dimethyl-9-oxo-3,7-diazabicyclo[3.3.1]-nonane-1,5-dicarboxylic acid dimethyl ester L[7]: Following the general bispidine synthesis, piperidone pL[7] (3.50 g, 6.5 mmol), formaldehyde solution (1.16 mL, 15.6 mmol), and 41% aqueous methylamine solution (0.66 mL, 7.8 mmol) in methanol (30 mL) gave the product in 50% yield. ^{1}H NMR ($CDCl_3$): δ = 2.10 (s, 3H, CH_3–N), 2.18 (s, 3H, CH_3–N), 2.46 (d, 2H, $^2J_{H,H}$ = 12.0 Hz, H6/H8 equatorial, CH_2), 2.77 (d, 2H, $^2J_{H,H}$ = 12.0 Hz, H6/H8 axial, CH_2), 3.89 (s, 6H, OCH_3), 4.74 (s, 2H, H2/H4, CH), 7.41 (dd, 2H, $^3J_{H,H}$ = 7.7 Hz, $^4J_{H,H}$ = 0.8 Hz, Ar–H), 7.66 (t, 2H, $^3J_{H,H}$ = 7.7 Hz, Ar–H), 8.01 ppm (dd, 2H, $^3J_{H,H}$ = 7.7 Hz, $^4J_{H,H}$ = 0.8 Hz, Ar–H); ^{13}C NMR ($CDCl_3$): δ = 43.6, 44.4 (2C, CH_3–N), 52.6 (2C, OCH_3), 60.7 (2C, CH_2–N), 61.8 (2C, C–CO), 73.0 (2C, CH–N), 121.9, 127.3, 138.7, 141.4, 160.3 (10C, C_{Ar}), 168.1 (2C, $COOCH_3$), 202.7 ppm (1C, C=O); MS-FAB (nibeol) m/z: 596.8 [M]; elemental analysis calcd (%): C 46.33, H 4.06, N 9.40; found: C 46.35 H 4.07 N 9.46.

3-Methyl-2,4-bis(pyridin-2-yl)-9-oxo-7-(quinolin-2-ylmethyl)-3,7-diazabicyclo[3.3.1]nonane-1,5-dicarboxylic acid dimethyl ester L[9]: Following the general bispidine synthesis, piperidone pL[1] (1.50 g, 3.9 mmol), formaldehyde solution (0.70 mL, 9.4 mmol), and 2-(aminomethyl)quinoline (0.74 g, 4.7 mmol) in methanol (15 mL) gave the product in 28% yield. ^{1}H NMR ($CDCl_3$): δ = 1.95 (s, 3H, CH_3–N), 2.81 (d, 2H, $^2J_{H,H}$ = 12.2 Hz, H6/H8 equatorial, CH_2), 3.25 (d, 2H, $^2J_{H,H}$ = 12.2 Hz, H6/H8 axial, CH_2), 3.47 (s, 2H, N–CH_2–Ar), 3.80 (s, 6H, OCH_3), 4.66 (s, 2H, H2/H4, CH), 6.90–7.20 (m, 4H, Ar–H), 7.50–7.85 (m, 3H, Ar–H), 7.90 (br d, 3H, $^3J_{H,H}$ = 7.6 Hz, Ar–H), 8.10–8.25 (m, 2H, Ar–H), 8.40 ppm (dd, 2H, $^3J_{H,H}$ = 4.9 Hz, $^4J_{H,H}$ = 1.0 Hz, Ar–H); ^{13}C NMR ($CDCl_3$): δ = 43.1 (1C, CH_3–N), 52.5 (2C, OCH_3), 62.4 (2C, C–CO), 64.0 (1C, N–CH_2–Ar), 73.7 (2C, CH–N), 122.4, 122.8, 123.8, 126.6, 127.3, 127.5, 129.5, 129.7, 136.0, 136.3, 147.9, 149.0, 157.6, 158.3 (14C, C_{Ar}), 168.5 ppm (2C, $COOCH_3$); MS-FAB (nibeol) m/z: 566.0 [M]; elemental analysis calcd (%): C 65.85, H 5.70, N 12.00; found: C 66.06, H 5.64, N 11.72.

2,4-Bis(6-bromopyridin-2-yl)-3-methyl-9-oxo-7-(pyridin-2-ylmethyl)-3,7-diazabicyclo[3.3.1]nonane-1,5-dicarboxylic acid dimethyl ester L[11]: Following the general bispidine synthesis, piperidone pL[7] (3.50 g, 6.5 mmol), formaldehyde solution (1.16 mL, 15.5 mmol), and 2-(aminomethyl)pyridine (0.80 mL, 7.8 mmol) in methanol (20 mL) gave the product in 35% yield. ^{1}H NMR ($CDCl_3$): δ = 2.03 (s, 3H, CH_3–N), 2.64 (d, 2H, $^2J_{H,H}$ = 12.5 Hz, H6/H8 equatorial, CH_2), 2.95 (d, 2H, $^2J_{H,H}$ = 12.5 Hz, H6/H8 axial, CH_2), 3.50 (s, 2H, N–CH_2–Ar), 3.87 (s, 6H, OCH_3), 4.68 (s, 2H, H2/H4, CH), 7.15–7.45 (m, 6H, Ar–H), 7.60–7.75 (m, 1H, Ar–H), 7.93 (dd, 2H, $^3J_{H,H}$ = 7.2 Hz, $^4J_{H,H}$ = 1.3 Hz, Ar–H), 8.71 ppm (br d, 2H, $^3J_{H,H}$ = 4.8 Hz, Ar–H); ^{13}C NMR ($CDCl_3$): δ = 43.5 (1C, CH_3–N), 52.6 (2C, OCH_3), 62.0 (2C, C–CO), 63.3 (1C, N–CH_2–Ar), 73.0 (2C, CH–N), 122.4, 122.5, 124.6, 127.1, 136.4, 138.6, 141.2, 149.7, 156.6, 159.7 (15C, C_{Ar}), 168.1 (2C, $COOCH_3$), 202.6 ppm (1C, C=O); MS-FAB (nibeol) m/z: 673.9 [M]; elemental analysis calcd (%): C 49.94, H 4.04, N 10.40; found: C 49.63, H 4.08, N 10.28.

3-Methyl-9-oxo-2,4-bis(quinolin-2-yl)-7-(quinolin-2-ylmethyl)-3,7-diazabicyclo[3.3.1]nonane-1,5-dicarboxylic acid dimethyl ester L[12]: Following the general bispidine synthesis, piperidone pL[12] (1.36 g, 2.8 mmol), formaldehyde solution (0.50 mL, 6.7 mmol) and 2-(aminomethyl)quinoline (0.53 g, 3.4 mmol) in methanol (15 mL) gave the product in 28% yield. ^{1}H NMR ($CDCl_3$): δ = 2.05 (s, 3H, CH_3–N), 2.80 (d, 2H, $^2J_{H,H}$ = 12.0 Hz, H6/H8 equatorial, CH_2), 3.22 (d, 2H, $^2J_{H,H}$ = 12.0 Hz, H6/H8 axial, CH_2), 3.76 (s, 2H, N–CH_2–Ar), 3.90 (s, 6H, OCH_3), 4.93 (s, 2H, H2/H4, CH), 7.40–8.40 ppm (m, 18H, Ar–H); ^{13}C NMR ($CDCl_3$): δ = 43.4 (1C, CH_3–N), 52.4 (2C, OCH_3), 62.6 (2C, C–CO), 63.9 (1C, N–CH_2–Ar), 74.1 (2C, CH–N), 121.0, 122.6, 126.5, 126.7, 127.3, 127.4, 127.5, 129.2, 129.4, 129.8, 136.0, 136.4, 147.4, 148.2, 157.3, 159.2 (27C, C_{Ar}), 168.4 (2C, $COOCH_3$), 203.3 ppm (1C, C=O); MS-FAB (nibeol) m/z: 666.1 [M]; elemental analysis calcd (%): C 71.20, H 5.38, N 10.38; found: C 70.95, H 5.25, N 10.33.

General (bispidine)copper(II) complex synthesis: To a solution of 1 equivalent of copper(II) tetrafluoroborate hexahydrate or copper(II) triflate in acetonitrile, one equivalent of the ligand was added and the mixture was stirred for 1 h at room temperature. The clean product was obtained by diethyl ether diffusion into the acetonitrile solution.

[CuL[1]](CF_3SO_3)$_2$·CH_3CN: Following the general procedure for metal complexes, L[1] (307 mg, 0.70 mmol) and $Cu(CF_3SO_3)_2$ (250 mg, 0.70 mmol) gave the product in 83% yield (490 mg); elemental analysis calcd: C 38.55 H 3.47, N 8.33, found: C 38.67, H 3.63, N 8.28.

[CuL[2]](BF_4)$_2$·3H_2O·CH_3CN: Following the general procedure for metal complexes, L[2] (115 mg (0.25 mmol) and $Cu(BF_4)_2$·6 H_2O (85 mg, 0.25 mmol) gave the product in 88% yield (175 mg); elemental analysis calcd: C 40.60, H 4.92, N 8.77; found: C 41.04, H 4.83, N 8.78; MS-FAB (nibeol) m/z: 566.1 [LCu·2H_2O], 547.0 [LCu·H_2O]. CV: $E_{1/2}$ (CH_3CN) = −410 mV, ΔE = 110 mV, $i_c^{p\prime}i_a^{p}$ = 2.55. UV (CH_3CN): λ (ε) = 624 (122), 920 nm (25 L cm^{-1} mol^{-1}); EPR (DMF/H_2O 3:2): $g_\parallel$ = 2.260 ($A_\parallel$ = 171 G), $g_\perp$ = 2.054 ($A_\perp$ = 10 G).

[CuL[3]](BF_4)$_2$·3H_2O·CH_3CN: Following the general procedure for metal complexes, L[3] (117 mg, 0.23 mmol)and $Cu(BF_4)_2$·6H_2O (81 mg, 0.23 mmol) gave the product in 73% yield (144 mg); elemental analysis calcd: C 39.03, H 4.73, N 8.43; found: C 39.39, H 4.66, N 8.12; MS-FAB (nibeol) m/z: 597.9 [LCu·2H_2O], 579.1 [LCu·H_2O]; CV: $E_{1/2}$ (CH_3CN) = −387 mV, ΔE = 94 mV, $i_c^{p\prime}i_a^{p}$ = 3.03; UV (CH_3CN): λ = 627 nm (ε = 127 L cm^{-1} mol^{-1}), λ = 929 nm (ε = 27 L cm^{-1} mol^{-1}); EPR (DMF/H_2O 3:2): $g_\parallel$ = 2.260 ($A_\parallel$ = 173 G), $g_\perp$ = 2.056 ($A_\perp$ = 9 G).

[CuL[4]](BF_4)$_2$·3H_2O·CH_3CN: Following the general procedure for metal complexes, L[4] (200 mg (0.34 mmol) and $Cu(BF_4)_2$·6H_2O (116 mg (0.34 mmol) gave the product in 85% yield (270 mg); elemental analysis calcd: C 32.34, H 3.58, N 7.54; found: C 32.13, H 3.47, N 7.34; MS-FAB (nibeol) m/z: 711.6 [LCu·3H_2O], 675.1 [LCu·H_2O]; CV: $E_{1/2}$ (CH_3CN) = −272 mV, ΔE = 77 mV, $i_c^{p\prime}i_a^{p}$ = 1.42; UV (CH_3CN): λ = 633 nm (ε = 129 L cm^{-1} mol^{-1}), λ = 970 nm (ε = 30 L cm^{-1} mol^{-1}); EPR (DMF/H_2O 3:2): $g_\parallel$ = 2.268 ($A_\parallel$ = 171 G), $g_\perp$ = 2.060 ($A_\perp$ = 10 G).

[CuL[5]](CF_3SO_3)$_2$·CH_3CN: Following the general procedure for metal complexes, L[5] (327 mg, 0.70 mmol) and $Cu(CF_3SO_3)_2$ (250 mg, 0.70 mmol) gave the product in 82% yield (510 mg); elemental analysis calcd: C 39.26, H 3.98, N 7.89, found: C 38.78, H 4.03, N 7.30.

[CuL[6]](BF_4)$_2$·3H_2O: Following the general procedure for metal complexes, L[6] (200 mg, 0.33 mmol) and $Cu(BF_4)_2$·6 H_2O (114 mg, 0.33 mmol) gave the product in 81% yield (240 mg); elemental analysis calcd: C 41.43, H 3.81, N 6.23; found: C 41.85, H 3.89, N 6.34; MS-FAB (nibeol) m/z: 707.8 [LCu·2H_2O], 688.8 [LCu·H_2O]; CV: $E_{1/2}$ (CH_3CN) = +17 mV, ΔE = 85 mV, $i_c^{p\prime}i_a^{p}$ = 1.30; UV (CH_3CN): λ = 735 nm (ε = 99 L cm^{-1} mol^{-1}), λ = 1030 nm (ε = 57 L cm^{-1} mol^{-1}).

[CuL[7]](BF_4)$_2$·3H_2O·CH_3CN: Following the general procedure for metal complexes, L[7] (200 mg, 0.34 mmol) and $Cu(BF_4)_2$·6H_2O (116 mg, 0.34 mmol) gave the product in 86% yield (271 mg); elemental analysis calcd: C 32.34, H 3.58, N 7.54; found: C 32.15, H 3.50, N 7.18; MS-FAB (nibeol) m/z: 676.6 [LCu·H_2O]; CV: $E_{1/2}$ (CH_3CN) = +56 mV, ΔE = 171 mV, $i_c^{p\prime}i_a^{p}$ = 1.07. UV (CH_3CN): λ = 660 nm (ε = 52 L cm^{-1} mol^{-1}), λ = 1091 nm (ε = 30 L cm^{-1} mol^{-1}); EPR (DMF/H_2O 3:2): $g_\parallel$ = 2.305 ($A_\parallel$ = 156 G), $g_\perp$ = 2.065 ($A_\perp$ = 10 G).

[CuL[7]](CF_3SO_3)$_2$·2CH_3CN: Following the general procedure for metal complexes, L[7] (880 mg, 1.40 mmol) and $Cu(CF_3SO_3)_2$ (500 mg, 1.40 mmol) gave the product in 85% yield (1.26 g); elemental analysis calcd: C 32.92, H 3.05, N 7.94; found: C 32.78, H 3.25, N 7.91.

[CuL[8]](CF_3SO_3)$_2$: Following the general procedure for metal complexes, L[8] (258 mg, 0.50 mmol) and $Cu(CF_3SO_3)_2$ (181 mg, 0.50 mmol) gave the product in 96% yield (420 mg); elemental analysis calcd: C 41.07, H 3.33, N 7.98; found: C 40.92, H 3.44, N 7.90.

[CuL[9]](BF_4)$_2$·4H_2O: Following the general procedure for metal complexes, L[9] (164 mg, 0.29 mmol)and $Cu(BF_4)_2$·6H_2O (100 mg, 0.29 mmol) gave the product in 89% yield (225 mg); elemental analysis calcd: C 43.93, H 4.49, N 8.01; found: C 43.83, H 4.32, N 8.00; MS-FAB (nibeol) m/z: 664.8 [LCu·2H_2O], 645.8 [LCu·H_2O]; CV: $E_{1/2}$ (CH_3CN) = −552 mV, ΔE = 70 mV, $i_c^{p\prime}i_a^{p}$ = 1.15; UV (CH_3CN): λ = 630 nm (ε = 132 L cm^{-1} mol^{-1}), λ = 881 nm (ε = 60 L cm^{-1} mol^{-1}); EPR (DMF/H_2O 3:2): $g_\parallel$ = 2.198 ($A_\parallel$ = 173 G), $g_\perp$ = 2.042 ($A_\perp$ = 25 G).

[CuL[10]](CF_3SO_3)$_2$·1.5CH_3CN: Following the general procedure for metal complexes, L[10] (258 mg, 0.50 mmol) and $Cu(CF_3SO_3)_2$ (181 mg, 0.50 mmol) gave the product in 82% yield (390 mg); elemental analysis calcd: C 41.42, H 3.73, N 9.51; found: C 41.56, H 3.99, N 9.37.

$[CuL^{11}](BF_4)_2\cdot 3H_2O$: Following the general procedure for metal complexes, L^{11} (157 mg, 0.23 mmol) and $Cu(BF_4)_2\cdot 6H_2O$ (80 mg, 0.23 mmol) gave the product in 89% yield (198 mg); elemental analysis calcd: C 34.87, H 3.45, N 7.26; found: C 34.85, H 3.66, N 7.26; MS-FAB (nibeol) m/z: 772.8 [LCu·2H_2O], 753.8 [LCu·H_2O]; CV: $E_{1/2}$ (CH_3CN) = −389 mV, ΔE = 75 mV, i_c^p/i_a^p = 1.16; UV (CH_3CN): λ = 642 nm (ε = 73 L cm^{-1} mol^{-1}), λ = 957 nm (ε = 16 L cm^{-1} mol^{-1}); EPR (DMF/H_2O 3:2): $g_\parallel$ = 2.258 ($A_\parallel$ = 168 G), $g_\perp$ = 2.055 ($A_\perp$ = 10 G).

$[CuL^{12}](BF_4)_2\cdot 5H_2O$: Following the general procedure for metal complexes, L^{12} (106 mg, 0.16 mmol) and $Cu(BF_4)_2\cdot 6H_2O$ (55 mg, 0.16 mmol) gave the product in 88% yield (140 mg); elemental analysis calcd: C 48.38, H 4.57, N 7.05; found: C 47.96, H 4.10, N 6.86; MS-FAB (nibeol) m/z: 764.9 [LCu·2H_2O], 745.9 [LCu·H_2O]; CV: $E_{1/2}$ (CH_3CN) = −35 mV, ΔE = 69 mV, i_c^p/i_a^p = 1.04; UV (CH_3CN): λ = 632 nm (ε = 125 L cm^{-1} mol^{-1}), λ = 710 nm (ε = 133 L cm^{-1} mol^{-1}), λ = 1091 nm (ε = 94 L cm^{-1} mol^{-1}); EPR (DMF/H_2O 3:2): $g_\parallel$ = 2.288 ($A_\parallel$ = 150 G), $g_\perp$ = 2.060 ($A_\perp$ = 6 G).

$[CuL^{12}](CF_3SO_3)_2\cdot CH_3CN$: Following the general procedure for metal complexes, L^{12} (200 mg, 0.30 mmol) and $Cu(CF_3SO_3)_2$ (109 mg, 0.30 mmol) gave the product in 73% yield (230 mg); elemental analysis calcd: C 48.25, H 3.57, N 6.70; found: C 48.25, H 3.58, N 6.57.

Aziridination experiments: Standard conditions: The catalyst (0.02 mmol, 5 mol% vs. PhINTs) was dissolved in dry, degassed acetonitrile (2 mL) under argon. Styrene (1 mL, 8.7 mmol, 22 equiv. vs. PhINTs) was stirred for 5 min over molecular sieves under argon and added subsequently to the catalyst solution. PhINTs (150 mg, 0.4 mmol, 1 equiv) was added and the mixture was stirred at 25 °C until all the PhINTs disappeared. The clear solution was filtered over neutral alumina, the alumina was washed with ethyl acetate (20 mL) and all solvents were removed in vacuo. The residue was dissolved in $CDCl_3$. The yield of aziridine product was determined by ^{1}H NMR spectroscopy versus anthrone (38.8 mg, 0.2 mmol). For the water-free complexes, triflate salts were used and the reactions were performed under standard conditions but with the addition of molecular sieves (4 Å). All experiments were performed in at least in duplicate.

Crystallography: Crystal data and details of the structure determinations are listed in Table 5. Intensity data were collected at low temperature with a Bruker AXS Smart 1000 CCD diffractometer and corrected for Lorentz, polarization, and absorption effects (semiempirical, SADABS).[53] The structures were solved by the heavy-atom method combined with structure expansion by direct methods applied to difference structure factors (DIRDIF)[54,55] and refined by full-matrix least squares methods based on F^2 with all measured unique reflections.[56] All non-hydrogen atoms were given anisotropic displacement parameters. Hydrogen atoms were input at calculated positions and refined with a riding model. The tetrafluoroborate anions were frequently found disordered. In such cases, split atom models were used and/or B−F and F···F distances were restrained to sensible values during refinement. In the case of $[(L^4)Cu(NCMe)][BF_4]_2$, disordered and partially occupied water of crystallization was removed from the structure (and the corresponding F_{obs}) with the SQUEEZE[57] procedure, as implemented in PLATON.[58] In the structure of $[(L^7)Cu(NCMe)_2][BF_4]_2$, the ligand Y on the copper atom could be modeled satisfactorily by a mixture of acetonitrile (occupancy 0.4) and water (occupancy 0.6) ligands. In addition, the keto group involving C9 of the bispidine ligand in this complex was found to have

Table 5. Details of the crystal structure determinations.

	$[(L^2)CuNCMe)]^{2+}$	$[(L^4)CuNCMe)]^{2+}$	$[(L^6)CuNCMe)]^{2+}$	$[(L^7)CuNCMe)]^{2+}$	$[(L^{12})CuNCMe)]^{2+}$
formula	$C_{27}H_{35}B_2CuF_8N_5O_6\cdot 2H_2O$	$C_{25}H_{29}B_2Br_2CuF_8N_5O_6$	$C_{35}H_{34}B_2Cl_2CuF_8N_6O_6\cdot CH_3CN$	$C_{26.8}H_{33.37}B_2Br_2CuF_8N_{5.4}O_{6.6}\cdot 0.84\,CH_3CN$	$C_{42}H_{40}B_2CuF_8N_6O_6$
crystal system	triclinic	monoclinic	monoclinic	triclinic	triclinic
space group	$P\bar{1}$	$C2/c$	$P2_1/c$	$P\bar{1}$	$P\bar{1}$
a [Å]	11.7884(6)	21.582(3)	15.4862(13)	11.4213(11)	11.0938(8)
b [Å]	11.8821(6)	11.8963(11)	13.0418(11)	12.2657(12)	13.1601(9)
c [Å]	13.9001(7)	26.109(2)	22.7423(16)	14.4043(14)	14.6098(11)
α [°]	107.6020(10)	90	90	101.286(2)	84.469(2)
β [°]	105.5540(10)	104.604(3)	118.594(4)	99.822(2)	80.1140(10)
γ [°]	105.9100(10)	90	90	110.684(2)	74.1640(10)
V [Å^{-3}]	1648.69(14)	6486.8(11)	4033.0(6)	1787.0(3)	2018.8(3)
Z	2	8	4	2	2
M_r	798.79	892.51	967.8	968.14	961.96
ρ_{calcd} [Mg m^{-3}]	1.609	1.828	1.594	1.799	1.583
F_{000}	822	3544	1972	968	986
$\mu(Mo_{K\alpha})$ [mm^{-1}]	0.764	3.232	0.765	2.943	0.637
transmission factors (max, min)	0.8320, 0.8032	0.7234, 0.5529	0.8318, 0.8318	0.7458, 0.4851	0.9381, 0.8420
λ [Å]	$Mo_{K\alpha}$, graphite monochromated, 0.71073				
T [K]	100(2)				
ϑ range [°]	1.7 to 32.0	1.6 to 27.1	1.5 to 32.0	1.9 to 25.7	1.6 to 27.5
index ranges	$-17\le h\le 16$ $-17\le k\le 16$ $0\le l\le 20$	$-27\le h\le 26$ $0\le k\le 15$ $0\le l\le 33$	$-23\le h\le 22$ $-19\le k\le 0$ $-32\le l\le 21$	$-13\le h\le 13$ $-14\le k\le 14$ $0\le l\le 17$	$-14\le h\le 14$ $-16\le k\le 17$ $0\le l\le 18$
reflns meas.	29595	82753	100717	30758	39144
unique, R_{int}	11209, 0.0297	7162 , 0.0728	13582 , 0.0620	6775, 0.0565	9250 , 0.0624
observed [$(I\ge 2\sigma(I)$]	9612	5741	9578	4798	6865
parameters refined	470	449	599	528	611
R indices (all data)					
$R1$	0.0432	0.0895	0.0691	0.0773	0.0689
w$R2$	0.1033	0.1603	0.1170	0.1542	0.1317
R indices [$I>2\sigma(I)$]					
$R1$	0.0352	0.0717	0.0434	0.0513	0.0478
w$R2$	0.0996	0.1531	0.1062	0.1416	0.1223
GOF on F^2	1.20	1.13	1.08	1.13	1.08
largest residual peaks [e Å^{-3}]	0.646, −0.347	1.120, −1.386	1.164, −0.569	2.281, −1.098	2.021, −0.580

been converted into a C(OH)(OMe) moiety, with the methyl group disordered over two positions. In the structure of $[(L^6)Cu(NCMe)_2][BF_4]_2$, the bispidine ligand was mainly present in its keto form (92%) with a small admixture of the diol (8%). All other complexes had the bispidine ligand exclusively in the diol form.

CCDC-666831, CCDC-666832, CCDC-666833, CCDC-666834, and CCDC-666835 contain the supplementary crystallographic data for this paper. These data can be obtained free of charge from The Cambridge Crystallographic Data Center via www.ccdc.cam.ac.uk/data_request/cif

Computational details: DFT calculations were performed with software packages Gaussian03,[59] Jaguar 5.5,[60] and ADF.[61] G03 was used for the geometry optimization and frequency calculations. Jaguar was used for pre-optimization and to perform PES scans to locate a few problematic/tricky species such as transitions states on the singlet surfaces. ADF was used for the geometry optimization and the energy decomposition analysis (EDA). Two different basis sets were used in G03; BS I was the combination of LanL2DZ[62–65] for Cu and a 6–31G basis set[66] for the other atoms. BS II used was the Ahlrichs TZVP basis set[67,68] For the location of transition states, either the normal transition state search with a starting geometry obtained from B3LYP[69,70]/BS I in G03 or the synchronous transit-guided quasi-Newton (STQN) method implemented in Gaussian 03 or a combination of both have been used. Frequency calculations were performed on all the optimized structures to verify their nature and to obtain the zero-point corrections to the energies. Unless otherwise stated, all the DFT energies and spin densities quoted herein are B3LYP/TZVP (BS II), including zero-point and free-energy corrections (enthalpy and entropy).

Acknowledgements

Generous financial support by the German Science Foundation (DFG) is gratefully acknowledged.

[1] M. Costas, M. P. Mehn, M. P. Jensen, L. Que, Jr., *Chem. Rev.* **2004**, *104*, 939.
[2] W. Nam, *Acc. Chem. Res.* **2007**, *40*, 522.
[3] K. Muniz-Fernandez in *Transition Metals in Organic Synthesis, 2nd Ed.*, *Vol. 2* (Eds.: M. Beller, C. Bolm), Wiley-VCH, Weinheim, Germany, **2004**, pp. 298.
[4] H. C. Kolb and K. B. Sharpless in *Transition Metals for Organic Synthesis, 2nd Ed.*, *Vol. 2* (Eds.: M. Beller, C. Bolm), Wiley-VCH, Weinheim, Germany, **2004**, pp. 275.
[5] E. N. Jacobsen, M. H. Wu in *Comprehensive Asymmetric Catalysis I–II, Vol. 2* (Eds.: E. N. Jacobsen, A. Pfaltz, Y. Hisashi), Springer, Berlin, Germany, **1999**, pp. 649.
[6] D. Tanner, *Angew. Chem.* **1994**, *106*, 625; *Angew. Chem. Int. Ed. Engl.* **1994**, *33*, 599.
[7] H. C. Kolb, M. G. Finn, K. B. Sharpless, *Angew. Chem.* **2001**, *113*, 2056; *Angew. Chem. Int. Ed.* **2001**, *40*, 2004.
[8] A. Yudin, *Aziridines and Epoxides in Organic Synthesis*, Wiley-VCH, Weinheim, Germany, **2006**.
[9] R. S. Coleman, J.-S. Kong, *J. Am. Chem. Soc.* **1998**, *120*, 3538.
[10] J. B. Sweeney, *Chem. Soc. Rev.* **2002**, *31*, 247.
[11] S.-M. Au, J. S. Huang, W.-Y. Yu, W.-H. Fung, C.-M. Che, *J. Am. Chem. Soc.* **1999**, *121*, 9120.
[12] J.-L. Liang, J.-S. Huang, X.-Q. Yu, N. Zhu, C.-M. Che, *Chem. Eur. J.* **2002**, *8*, 1563.
[13] D. A. Evans, M. M. Faul, M. T. Bilodeau, *J. Org. Chem.* **1991**, *56*, 6744.
[14] D. A. Evans, M. M. Faul, M. T. Bilodeau, *J. Am. Chem. Soc.* **1994**, *116*, 2742.
[15] Y. Yamada, T. Yamamoto, M. Okawara, *Chem. Lett.* **1975**, 361.
[16] T. P. Albone, P. S. Aujnla, P. C. Taylor, S. Challenger, A. M. Derrick, *J. Org. Chem.* **1998**, *63*, 9569.
[17] M. M. Diaz-Requejo, P. J. Perez, M. Brookhart, J. L. Templeton, *Organometallics* **1997**, *16*, 4399.
[18] P. Brandt, M. J. Södergren, P. G. Andersson, P.-O. Norrby, *J. Am. Chem. Soc.* **2000**, *122*, 8013.
[19] P. Müller, C. Baud, Y. Jacquier, *Can. J. Chem.* **1998**, *76*, 738.
[20] K. M. Gillespie, E. J. Crust, R. J. Deeth, P. Scott, *Chem. Commun.* **2001**, 785.
[21] P. Comba, M. Kerscher, W. Schiek, *Prog. Inorg. Chem.* **2007**, *55*, 613.
[22] P. Comba, C. Lopez de Laorden, H. Pritzkow, *Helv. Chim. Acta* **2005**, *88*, 647.
[23] H. Börzel, P. Comba, K. S. Hagen, C. Katsichtis, H. Pritzkow, *Chem. Eur. J.* **2000**, *6*, 914.
[24] F. Mohr, S. A. Binfield, J. C. Fettinger, A. N. Vedernikow, *J. Org. Chem.* **2005**, *70*, 4833.
[25] P. Comba, M. Kerscher, M. Merz, V. Müller, H. Pritzkow, R. Remenyi, W. Schiek, Y. Xiong, *Chem. Eur. J.* **2002**, *8*, 5750.
[26] P. Comba, W. Schiek, *Coord. Chem. Rev.* **2003**, *238–239*, 21.
[27] K. Born, P. Comba, R. Ferrari, S. Kuwata, G. A. Lawrance, H. Wadepohl, *Inorg. Chem.* **2007**, *46*, 458.
[28] P. Brandt, T. Norrby, B. Akermark, P.-O. Norrby, *Inorg. Chem.* **1998**, *37*, 4120.
[29] C. Mannich, P. Mohs, *Chem. Ber. B* **1930**, *63*, 608.
[30] P. Comba, M. Merz, H. Pritzkow, *Eur. J. Inorg. Chem.* **2003**, 1711.
[31] H. A. Goodwin, F. Lions, *J. Am. Chem. Soc. J. Am. Chem.Soc.* **1959**, *81*, 6415.
[32] X. Wang, P. Rabbat, P. O'Shea, R. Tillyer, E. J. J. Grabowski, P. J. Reider, *Tetrahedron Lett.* **2000**, *41*, 4335.
[33] M. Adamczyk, R. E. Reddy, *Tetrahedron: Asymmetry* **2001**, *12*, 1047.
[34] W. M. Tadros, H. A. Shoeb, M. A. Kira, F. Yousif, E. M. Ekladios, S. A. Ibrahim, *Indian J. Chem.* **1975**, *13*, 1366.
[35] H. Börzel, P. Comba, C. Katsichtis, W. Kiefer, A. Lienke, V. Nagel, H. Pritzkow, *Chem. Eur. J.* **1999**, *5*, 1716.
[36] P. Comba, B. Martin, A. Prikhod'ko, H. Pritzkow, H. Rohwer, *Comptes Rendus Chimie* **2005**, *6*, 1506.
[37] P. Comba, A. Hauser, M. Kerscher, H. Pritzkow, *Angew. Chem.* **2003**, *115*, 4675; *Angew. Chem. Int. Ed.* **2003**, *42*, 4536.
[38] P. Comba, M. Kerscher, *Cryst. Eng.* **2004**, *7*, 197.
[39] P. Comba, *Coord. Chem. Rev.* **1999**, *182*, 343.
[40] Redox potentials and ligand field strengths are known to be correlated, and from ligand field theory there also emerges a correlation of dd transitions and spin Hamiltonian parameters.[59]
[41] Note that the co-ligands are not identical in all structural, spectroscopic, and electrochemical experiments, neither are they in the aziridination experiments described; note also that the substituents of the aromatic rings also lead to a variation of the nucleophilicity of the donors, and this obviously also influences the relative stability of the three possible Jahn–Teller isomers.
[42] J. A. Halfen, J. K. Hallman, J. A. Schultz, J. P. Emerson, *Organometallics* **1999**, *18*, 5435.
[43] Usually, (bispidine)copper(II) complexes contain coordinated or crystal water owing to their syntheses; also, these complexes are usually very hygroscopic.
[44] T. Dhanalakshmi, E. Suresh, H. Stoeckli-Evans, M. Palaniandavar, *Eur. J. Inorg. Chem.* **2006**, 4687.
[45] Z. Li, R. W. Quan, E. N. Jacobsen, *J. Am. Chem. Soc.* **1995**, *117*, 5889.
[46] Y. M. Badiei, A. Krishnaswamy, M. M. Melzer, T. Warren, *J. Am. Chem. Soc.* **2006**, *128*, 15056.
[47] R. W. Quan, Z. Li, E. N. Jacobsen, *J. Am. Chem. Soc.* **1996**, *118*, 8156.
[48] Note that $^3C_{N7}$ is lower in energy than $^1C_{N3}$. However, there are appreciable deviations in the structures of the two isomers and $^3C_{N7}$ is 3.3 kJ mol^{-1} higher in energy than $^3C_{N3}$. Moreover the product of $^3C_{N7}$, $^1D_{N7}$ is almost 20 kJ mol^{-1} higher in energy than $^1D_{N3}$. Therefore, the path starting with $^3C_{N7}$ is neglected.
[49] K. Born, P. Comba, M. Kerscher, H. Rohwer, unpublished results.

[50] K. Born, P. Comba, A. Daubinet, A. Fuchs, H. Wadepohl, *J. Biol. Inorg. Chem.* **2007**, *12*, 36.
[51] D. Wang, G. R. Hanson, *J. Magn. Reson. Ser. A* **1995**, *117*, 1.
[52] D. Wang, G. R. Hanson, *Appl. Magn. Reson.* **1996**, *11*, 401.
[53] G. M. Sheldrick in SADABS 2004–2007, Bruker AXS, Göttingen, **2004–2007**.
[54] V. Parathasarathi, *Acta. Crystallog. Sect. A* **1983**, *39*, 860.
[55] P. T. Beurskens, G. Beurskens, R. de Gelder, S. G. Ganda, R. O. Gould, R. Israel, J. M. M. Smits in DIRDIF-99, University of Nijmegen, The Netherlands, **1999**.
[56] G. M. Sheldrick in SHELXS-97 Program for structure solution; SHELXL-97 Program for structure refinement, University of Göttingen, Göttingen, **1997**.
[57] P. van der Sluis, A. L. Spek, *Acta Crystallogr. Sect. A* **1990**, *46*, 194.
[58] A. L. Spek, *J. Appl. Crystallogr.* **2003**, *36*, 7.
[59] Gaussian 03, Revision B.03, M. J. Frisch, G. W. Trucks, H. B. Schlegel, G. E. Scuseria, M. A. Robb, J. R. Cheeseman, J. A. Montgomery, Jr., T. Vreven, K. N. Kudin, J. C. Burant, J. M. Millam, S. S. Iyengar, J. Tomasi, V. Barone, B. Mennucci, M. Cossi, G. Scalmani, N. Rega, G. A. Petersson, H. Nakatsuji, M. Hada, M. Ehara, K. Toyota, R. Fukuda, J. Hasegawa, M. Ishida, T. Nakajima, Y. Honda, O. Kitao, H. Nakai, M. Klene, X. Li, J. E. Knox, H. P. Hratchian, J. B. Cross, V. Bakken, C. Adamo, J. Jaramillo, R. Gomperts, R. E. Stratmann, O. Yazyev, A. J. Austin, R. Cammi, C. Pomelli, J. W. Ochterski, P. Y. Ayala, K. Morokuma, G. A. Voth, P. Salvador, J. J. Dannenberg, V. G. Zakrzewski, S. Dapprich, A. D. Daniels, M. C. Strain, O. Farkas, D. K. Malick, A. D. Rabuck, K. Raghavachari, J. B. Foresman, J. V. Ortiz, Q. Cui, A. G. Baboul, S. Clifford, J. Cioslowski, B. B. Stefanov, G. Liu, A. Liashenko, P. Piskorz, I. Komaromi, R. L. Martin, D. J. Fox, T. Keith, M. A. Al-Laham, C. Y. Peng, A. Nanayakkara, M. Challacombe, P. M. W. Gill, B. Johnson, W. Chen, M. W. Wong, C. Gonzalez, J. A. Pople, Gaussian, Inc., Wallingford CT, **2004**.
[60] *JAGUAR 5.5*, Schrödinger, Inc., Portland, OR.
[61] A. Bérces et al. in ADF2004.01 SCM, Theoretical Chemistry, Vrije Universiteit: Amsterdam, The Netherlands, **2004**.
[62] T. H. Dunning, Jr., P. J. Hay in *Modern Theoretical Chemistry, Vol. 3*, (Ed. E. H. F. Schaefer III, Plenum Press, New York, **1976**, pp. 1.
[63] P. J. Hay, W. R. Wadt, *J. Chem. Phys.* **1985**, *82*, 270.
[64] W. R. Wadt, P. J. Hay, *J. Chem. Phys.* **1985**, *82*, 284.
[65] P. J. Hay, W. R. Wadt, *J. Chem. Phys.* **1985**, *82*, 299.
[66] R. Ditchfield, W. J. Hehre, J. A. Pople, *J. Chem. Phys.* **1971**, *54*, 724.
[67] A. Schäfer, H. Horn, R. Ahlrichs, *J. Chem. Phys.* **1992**, *97*, 2571.
[68] A. Schäfer, C. Huber, R. Ahlrichs, *J. Chem. Phys.* **1994**, *100*, 5829.
[69] C. Lee, W. Yang, R. G. Parr, *Phys. Rev. B* **1988**, *37*, 785.
[70] A. D. Becke, *J. Chem. Phys.* **1993**, *98*, 5648.

Received: December 4, 2007
Revised: February 7, 2008
Published online: April 22, 2008

